TIME–FREQUENCY AND COORDINATE–MOMENTUM WIGNER WAVEPACKETS IN NONLINEAR SPECTROSCOPY

S. MUKAMEL, C. CIORDAS-CIURDARIU, AND V. KHIDEKEL

Department of Chemistry
University of Rochester
Rochester, New York

CONTENTS

I. INTRODUCTION

In the analysis of linear and nonlinear optical spectroscopies, the electric fields and optical gates are commonly represented by their amplitudes. Similarly, the material system is represented by an amplitude as well, the wave function. However, optical signals are given by products of such amplitudes.

Advances in Chemical Physics, Volume 101: Chemical Reactions and Their Control on the Femtosecond Time Scale, XXth Solvay Conference on Chemistry, Edited by Pierre Gaspard, Irene Burghardt, I. Prigogine, and Stuart A. Rice.
ISBN 0-471-18048-3

For the material system we need two amplitudes, representing the bra and ket used in the calculation of the polarization matrix element, whereas the number of field amplitudes depends on the order of the particular nonlinear process. An improved intuitive picture can be obtained by grouping the field amplitudes in pairs using a mixed temporal–spectral (Wigner) representation. This often highlights much more clearly the roles of spectral and temporal features of the field and provides valuable information about the signal (e.g., its time-dependent spectrum). Similarly, the pair of wave function amplitudes can be used to form the density matrix, and a Wigner transform with respect to space brings it to a mixed coordinate–momentum (phase-space) representation that closely resembles the classical phase-space distribution.* In this chapter we show how such mixed Wigner representations can be used effectively to compute and interpret optical signals.

The development of a mixed time–frequency representation in which both characteristics of the field and the response function are highlighted is currently receiving considerable attention. This activity is triggered by the rapid progress in pulse-shaping techniques, which made it possible to control the temporal profiles as well as the phases of optical fields with a remarkable accuracy [1–4]. These developments have further opened up the possibility of coherent control of dynamics in condensed phases [5–7].

Mixed time–frequency measurements were first introduced in acoustics in the analysis of sound and speech [8]. The frequency-resolved optical gating (FROG) technique [9, 10] enables one to measure the FROG spectrograms that contain both temporal and spectral information about the signal. This spectrogram can then be inverted, and the intensity and phase of a pulse is obtained. However, the correspondence between FROG signals and the temporal and spectral profiles of the field is not always unique [7, 9].

In this chapter we use the Wigner distribution, known also as the chronocyclic representation [11–15]. The interest in using this distribution, whose properties have been known for a long time, for the description of optical fields was resuscitated in the last few years, when it became apparent that it not only is a theoretical construct but also can be actually retrieved from nonlinear experiments [12], providing, therefore, a method for characterizing a signal completely, both in the time and frequency domain. The easiest way to obtain a mixed time–frequency picture (spectrogram) is to pass the signal through a spectral and temporal filter centered at some controlled frequency and time prior to its detection [16].

Phase-space wavepackets for nuclear motions have been applied to the interpretation of nonlinear optical measurements using the Liouville space

*The electric field can also be transformed in coordinate space, but this will not be considered here.

representation of the response function [17]. We shall demonstrate how such wavepackets can be used in the analysis of fluorescence and pump–probe spectroscopies.

In Section II we study spontaneous light emission. We consider a setup in which the signal emitted by the sample passes through both a spectral and a temporal gate before it reaches the detector. We show that the detected signal can be written as a convolution of the bare autocorrelation function and a joint characteristic function of both gates. We then develop a correlation function expression for the bare signal and show that this expression is identical to but more compact than the one obtained by calculating the photon emission rate in Liouville space [17]. In Section III we rewrite the material response function in phase space using the Wigner representation for the external fields, the gate, and the doorway and window wavepackets. In Section IV we apply the same formalism to develop the doorway–window picture for pump–probe spectroscopy. Finally, in Section V we show how our pump–probe expressions may be generalized and applied to the calculation of heterodyne-detected four-wave mixing spectroscopies.

II. CORRELATION FUNCTION EXPRESSION FOR SPONTANEOUS LIGHT EMISSION

We consider a single molecule whose interaction with an external radiation field $E(\mathbf{r}, t)$ is given by

$$H_{\text{Int}} = -V \cdot E(\mathbf{r}, t) \tag{2.1}$$

where V is the molecular dipole operator and $\mathbf{r}$ is its position. (The following expressions hold for a real dilute sample made of noninteracting molecules. For simplifying the notation we consider a single molecule.)

While discussing the properties of light using a classical description, the formalism is recast as close as possible to the quantum form by introducing the complex analytical signal $\mathcal{E}(\mathbf{r}, t)$, which may be obtained from the real field $E(\mathbf{r}, t)$ by [18]

$$\mathcal{E}(\mathbf{r}, t) \equiv \frac{1}{2\pi} \int_0^\infty d\omega\, e^{-i\omega t} \int_{-\infty}^\infty E(\mathbf{r}, t') e^{i\omega t'}\, dt' \tag{2.2}$$

By construction, the Fourier transform of the analytical signal contains only positive frequencies. We further assume that the field comprises a finite number of pulses with wave vectors $\mathbf{k}_j$. We then have

$$E(\mathbf{r},t) = \sum_j \mathcal{E}_j(t)e^{i\mathbf{k}_j\mathbf{r}} + \text{c.c.}$$

$$P(\mathbf{r},t) = \sum_j \mathcal{P}_j(t)e^{i\mathbf{k}_j\mathbf{r}} + \text{c.c.}$$

where $\mathcal{E}_j(t)$ and $\mathcal{P}_j(t)$ are the complex-valued analytic field and polarization, respectively. The field envelopes $\mathcal{E}_j(t)$ can be further represented in the form $\mathcal{E}_j(t) = \tilde{\mathcal{E}}_j(t)e^{-i\omega_j t}$, where $\tilde{\mathcal{E}}_j(t)$ is a slowly-varying envelope and ω_j is the carrier frequency.

In the simplest (homodyne) detection scheme one measures the time-integrated intensity of the field generated by the sample in a given direction $\mathbf{k}_j$:

$$I(\mathbf{k}_j) \propto \int_{-\infty}^{\infty} \langle \mathcal{E}_j^*(t)\mathcal{E}_j(t)\rangle \, dt \tag{2.3}$$

Time-integrated detection is commonly used in wave-mixing experiments, such as photon echoes [19]. However, time-integrated photon echo signals do not contain sufficient information to establish the complete form of the spectral density responsible for optical dephasing [20]. Additionally, most valuable microscopic information may be obtained by time-gated (or time-resolved) detection [21, 22], achieved by overlapping the total response with a narrow gate pulse, which provides the temporal profile of the signal. A number of more elaborate techniques, which provide a richer information, including spectral characteristics of the signal, have been developed. The second-order autocorrelation function $\langle \mathcal{E}_j^*(t_1)\mathcal{E}_j(t_2)\rangle$ allows one to obtain more information about the field [18]: its amplitude as well as the phase. This can be viewed as the time-resolved spectrum of the light pulse, namely the time-dependent strength of its different frequency components.

The autocorrelation signal can be observed by passing the field through two gating devices, a spectral gate whose transmission function is centered at ω_0 and a time gate centered at t_0. The measured signal (the total energy received by the detector) is given by Eq. (2.3), except that $\mathcal{E}_j(t)$ now denotes the gated field $\overline{\mathcal{E}}_j$. The resulting *gated autocorrelation signal* becomes a function of both ω_0 and t_0, thus retaining its temporal and spectral information:

$$I_{\text{Auto}}(t_0,\omega_0) \propto \int_{-\infty}^{\infty} \langle \overline{\mathcal{E}}_j^*(t)\overline{\mathcal{E}}_j(t)\rangle \, dt \tag{2.4}$$

In Appendix A we show that the gated signal $I_{\text{Auto}}(t_0, \omega_0)$ can be recast in the form

$$I_{\text{Auto}}(t_0, \omega_0) = \int\int_{-\infty}^{\infty} \frac{dt\ d\omega}{2\pi}\, \Phi(t, \omega; t_0, \omega_0)\tilde{I}_{\text{Auto}}(t, \omega) \tag{2.5}$$

where

$$\tilde{I}_{\text{Auto}}(t, \omega) = \int_{-\infty}^{\infty} \langle \tilde{\mathcal{P}}^*(t - \tfrac{1}{2}\tau)\tilde{\mathcal{P}}(t + \tfrac{1}{2}\tau)\rangle e^{i\omega\tau}\, d\tau \tag{2.6}$$

is the ideal *(bare) autocorrelation signal*, corresponding to a gate with an infinite temporal and spectral resolution, and $\Phi(t', \omega'; t_0, \omega_0)$ is the joint gate function that depends on the transmission functions of both gates as well as the order in which they are applied. This function is calculated in Appendix A. The bare signal is not positive definite and it may even assume negative values. This is not the case for the gated signal, which is written as the squared amplitude (of the gated field) and is therefore guaranteed to be nonnegative. The gate function $\Phi(t', \omega'; t_0, \omega_0)$ is usually localized in both time and frequency. However, it cannot be made infinitely narrow in both variables due to fundamental uncertainty of the Fourier transform, $\Delta\omega\Delta t \geq 1$. It then follows that mathematically the ideal gate $\Phi(t, \omega; t_0, \omega_0) = \delta(t_0 - t) \times \delta(\omega_0 - \omega)$ cannot be realized. Physically, however, an ideal gate is possible when both the temporal and spectral profiles of the gate are narrower than certain relevant material scales. The detected signal is then virtually identical to the bare signal. An example of such a limiting case is the snapshot limit of pump–probe spectroscopy [17].

By expanding $\langle \tilde{\mathcal{P}}^*(t - \frac{1}{2}\tau)\tilde{\mathcal{P}}(t + \frac{1}{2})\rangle$ to second order in the external field, the autocorrelation signal $\tilde{I}_{\text{Auto}}(t, \omega)$ gives the spontaneous light emission, denoted $\tilde{I}_{\text{SLE}}(t, \omega)$. In Appendix C we express the polarization in terms of a response function convoluted with the external field. By invoking the rotating-wave approximation, we get

$$\begin{aligned}\tilde{I}_{\text{SLE}}(t, \omega) = \int_{-\infty}^{\infty} d\tau \int_0^{\infty} d\tau_1 \int_0^{\infty} d\tau_2 \\ F^{(4)}(t - \tau_1 + \tfrac{1}{2}\tau, t + \tfrac{1}{2}\tau, t - \tfrac{1}{2}\tau, t - \tau_2 - \tfrac{1}{2}\tau) \\ \times \mathcal{E}^*(t - \tau_1 + \tfrac{1}{2}\tau)\mathcal{E}(t - \tau_2 - \tfrac{1}{2}\tau)e^{i\omega t}\end{aligned} \tag{2.7}$$

where

$$F^{(4)}(t_1,t_2,t_3,t_4) \equiv \langle V(t_1)V(t_2)V(t_3)V(t_4)\rangle \tag{2.8}$$

is the four-point equilibrium correlation function of the dipole operator. $V(t)$ are operators in the interaction picture, evolving in time with respect to the material Hamiltonian H_0 (with no external field)

$$V(t) = \exp(iH_0t)V\exp(-iH_0t) \tag{2.9}$$

Hereafter we set $\hbar = 1$ (unless its inclusion is needed for clarity). The Liouville space path diagram corresponding to this correlation function is shown in Fig. 1.

An alternative way to calculate the SLE spectrum is to expand the molecular density matrix to second order in the field and compute the time-dependent photon emission rate. The resulting expression is [23]

$$\begin{aligned}\tilde{I}_{\mathrm{SLE}}(t',\omega) = &\int_0^\infty dt_1 \int_0^\infty dt_2 \int_0^\infty dt_3 \\ &\cdot \{e^{i\omega t_3}F^{(4)}(t'-t_3-t_2-t_1,t',t'-t_3,t'-t_3-t_2) \\ &\times \mathcal{E}(t'-t_1-t_2-t_3)\mathcal{E}^*(t'-t_2-t_3) \\ &+ e^{i\omega t_3}F^{(4)}(t'-t_3-t_2,t',t'-t_3,t'-t_3-t_2-t_1) \\ &\times \mathcal{E}^*(t'-t_1-t_2-t_3)\mathcal{E}(t'-t_2-t_3) \\ &+ e^{i\omega(t_3+t_2)}F^{(4)}(t'-t_3,t',t'-t_3-t_2,t'-t_3-t_2-t_1) \\ &\times \mathcal{E}^*(t'-t_1-t_2-t_3)\mathcal{E}(t'-t_3)\} + \text{c.c.}\end{aligned} \tag{2.10}$$

This formula, unlike Eq. (2.7), maintains a complete bookkeeping of the time ordering of the various interactions with the radiation field [17] and has six terms; the Liouville space paths corresponding to three of them are shown in Fig. 2, and the paths for the complex-conjugate terms are obtained by interchanging the left and the right portions of each path.

It can be easily shown that Eqs. (2.7) and (2.10) are identical. Indeed, the three-dimensional integration domain in (2.7) can be divided into six subdomains, each corresponding to a term of (2.10) upon a proper change of time variables:

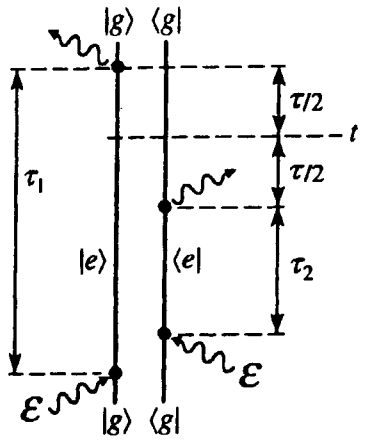

Figure 1. Liouville space diagram corresponding to the only term that contributes to the spontaneous light emission from a two-level system within the rotating-wave approximation [Eq. (2.7)]. Here $|g\rangle$ and $|e\rangle$ denote the ground and the excited states, respectively.

$$\int_{-\infty}^{\infty} d\tau \int_0^{\infty} d\tau_1 \int_0^{\infty} d\tau_2$$

$$= \int_0^{\infty} d\tau \int_0^{\infty} d\tau_2 \left[\int_0^{\tau} d\tau_1 + \int_{\tau}^{\tau+\tau_2} d\tau_1 + \int_{\tau+\tau_2}^{\infty} d\tau_1 \right]$$

$$+ \int_{-\infty}^{0} d\tau \int_0^{\infty} d\tau_1 \left[\int_0^{-\tau} d\tau_2 + \int_{-\tau}^{-\tau+\tau_1} d\tau_2 + \int_{-\tau+\tau_1}^{\infty} d\tau_2 \right] \tag{2.11}$$

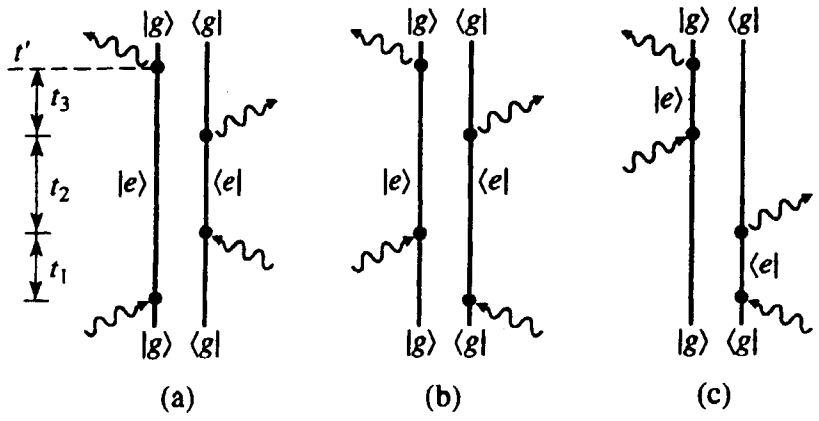

Figure 2. Liouville space paths for the three terms of Eq. (2.10).

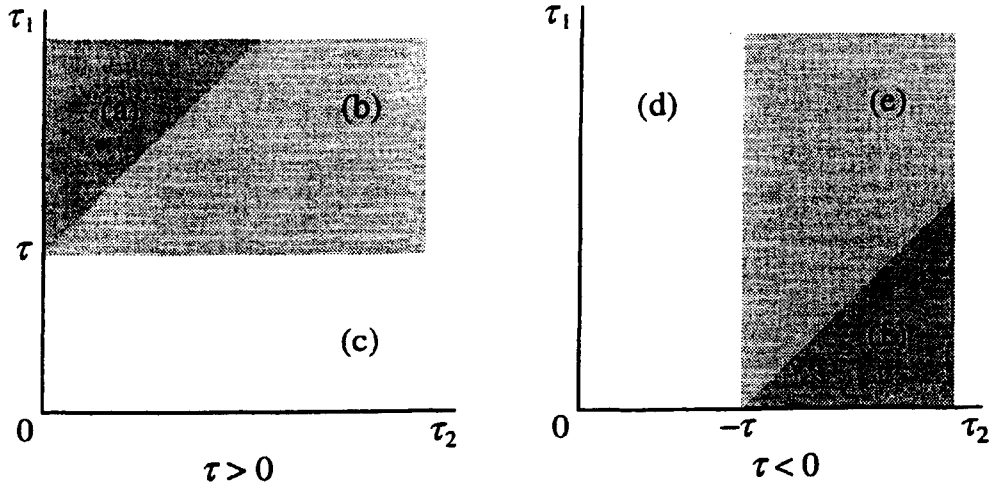

Figure 3. Diagrams showing how to divide the triple integral in (2.7) to get the six terms of (2.10). Domains (*a*), (*b*), and (*c*) correspond to the three Liouville space paths given in Fig. 2 and domains (*d*), (*e*), and (*f*) to the complex-conjugate paths.

These integration domains are depicted in Fig. 3. The first three terms in (2.11) represent the third, the second, and the first terms in (2.10), respectively. A simple substitution of time variables, as specified in Table I, finally recovers the six terms of (2.10).

We now rewrite Eq. (2.7) by introducing the Wigner distribution for the external field as well,

$$W_{\mathcal{E}}(t,\omega) = \int_{-\infty}^{\infty} \mathcal{E}^*(t - \tfrac{1}{2}\tau)\mathcal{E}(t + \tfrac{1}{2}\tau)e^{i\omega\tau}\, d\tau \tag{2.12}$$

Substituting (2.12) into (2.7), we obtain the autocorrelation signal (2.5), where the bare signal is given by

TABLE I
Correspondence between Time Arguments of Eq. (2.7) and Six Terms of Eq. (2.10)

Term	t	τ	τ_1	τ_2
(a)	$t' - \frac{1}{2}t_3$	t_3	$t_1 + t_2 + t_3$	t_2
(b)	$t' - \frac{1}{2}t_3$	t_3	$t_2 + t_3$	$t_1 + t_2$
(c)	$t' - \frac{1}{2}t_3$	$t_2 + t_3$	t_1	t_3
(d)	$t' - \frac{1}{2}t_3$	$-t_3$	t_2	$t_1 + t_2 + t_3$
(e)	$t' - \frac{1}{2}t_3$	$-t_3$	$t_1 + t_2$	$t_2 + t_3$
(f)	$t' - \frac{1}{2}t_3$	$-t_2 - t_3$	t_1	t_3

$$\tilde{I}_{\mathrm{SLE}}(t,\omega) = \frac{1}{2\pi}\int_{-\infty}^{\infty} d\tau \int_{0}^{\infty} d\tau_1 \int_{0}^{\infty} d\tau_2 \int_{-\infty}^{\infty} d\omega_1\, e^{i\omega\tau} e^{-i\omega_1(\tau_1-\tau_2-\tau)}$$
$$\times F^{(4)}\left(t-\tau_1+\tfrac{1}{2}\tau, t+\tfrac{1}{2}\tau, t-\tfrac{1}{2}\tau, t-\tau_2-\tfrac{1}{2}\tau\right)$$
$$\cdot \mathcal{W}_{\mathcal{E}}(t-\tfrac{1}{2}(\tau_1+\tau_2),\omega_1) \qquad (2.13)$$

We have thus expressed the autocorrelation signals using the Wigner representation for both the external fields and the gate. The molecular properties are contained in the response function $F^{(4)}$. In the next section, we show how when the incoming external pulses and the detection gate are temporally well separated, we can use the Wigner representation for the material system as well.

III. WIGNER WAVEPACKETS IN PHASE SPACE: THE DOORWAY–WINDOW PICTURE

Assuming that the incoming pulses and the gated emission are temporally well separated, we can recast the general expression for the SLE presented in the previous section in a different form that lends itself more easily to physical interpretation. This will allow us to separate the process into the preparation of a doorway wavepacket by the pump field, a subsequent propagation of this wavepacket for a specified period, and finally observing it through a window wavepacket created by the detection device. By using the Wigner phase-space function for the doorway and the window wavepackets, we obtain an "all-Wigner" representation of the signal.

We first rewrite Eq. (2.13) by making the following change of variables $\tau_1 + \tau_2 \rightarrow 2\tau'$, $\tau_1 - \tau_2 + \tau \rightarrow \tau''$. The assumption that the pulses are well separated temporally allows us to extend all time integrals to infinity, resulting in

$$\tilde{I}_{\mathrm{SLE}}(t,\omega) = \frac{1}{2\pi}\iint_{-\infty}^{\infty} d\tau\, d\tau'' \int_{0}^{\infty} d\tau' \int_{-\infty}^{\infty} d\omega_1\, e^{i\omega\tau} e^{i\omega_1\tau''}$$
$$F^{(4)}(t-\tau'+\tfrac{1}{2}\tau'', t+\tfrac{1}{2}\tau, t-\tfrac{1}{2}\tau, t-\tau'-\tfrac{1}{2}\tau'') \cdot \mathcal{W}_{\mathcal{E}}(t-\tau',\omega_1) \qquad (3.1)$$

By introducing a complete basis set in the coordinate representation, we show in Appendix D that the SLE signal can be recast in the form

$$I_{\mathrm{SLE}}(t_0,\omega_0)=\iint dx\ dx'\ W_e(xx';\omega_0)D_e(xx';t_0) \tag{3.2}$$

with

$$D_e(xx';t_0)=$$
$$\frac{1}{2\pi}\iiint_{-\infty}^{\infty} dt''\ d\tau''\ d\omega_1\ \mathcal{W}_{\mathcal{E}}(t'',\omega_1)e^{i\omega_1\tau''}$$
$$\times\langle x|e^{iH_e(\tau''/2-t''+t_0)}V_{eg}e^{-iH_g(\tau''/2)}\rho_0 e^{-iH_g(\tau''/2)}V_{ge}\cdot e^{iH_e(\tau''/2+t''-t_0)}|x'\rangle \tag{3.3}$$

$$W_e(xx';\omega_0)=\frac{1}{2\pi}\iiint_{-\infty}^{\infty} dt\ d\tau\ d\omega\ \Phi(t,\omega;0,\omega_0)e^{i\omega\tau}$$
$$\times\langle x|e^{-iH_e(\tau/2-t)}V_{eg}e^{iH_g\tau}V_{ge}e^{-iH_e(\tau/2+t)}|x'\rangle \tag{3.4}$$

Here $D_e(xx';0)$ is the *doorway wavepacket* representing the molecular density matrix created by the external field at $t''=0$. It then propagates for the delay period t_0 resulting in $D_e(xx';t_0)$. Here, $W_e(xx';\omega_0)$ is the *window wavepacket* created by the gate and represents the density matrix responsible for emission at frequency ω_0. (Note that the time delay evolution is included now in the doorway wavepacket so that the window does not depend on t_0.) The signal is obtained by calculating the overlap of these two wavepackets in Liouville space. A more intuitive picture of these wavepackets can be obtained by switching to the Wigner (phase-space) representation

$$A(pq)\equiv\iint_{-\infty}^{\infty} A(xx')e^{-ip(x-x')}\delta(x+x'-2q)\,dx\ dx' \qquad A=D_e,W_e$$

and the signal [Eq. (3.2)] assumes the form

$$I_{\mathrm{SLE}}(t_0,\omega_0)=\iint dp\ dq\ W_e(pq;\omega_0)D_e(pq;t_0) \tag{3.5}$$

Now the overlap of these wavepackets is calculated in phase space. Note that this is a fully quantum mechanical picture, and no classical approximations were made. Our only assumption is that the excitation and gating processes are well separated. This form, however, allows the development

of semiclassical approximations for computing the doorway and the window wavepackets. When the Wigner distributions of both the external field and the gate function are fast compared with the time scale of nuclear dynamics and have a narrow spectrum compared with the dephasing rate, we can set $W_{\mathcal{E}}(t'', \omega_1) \approx \delta(t'') \cdot \delta(\omega_1 - \omega_\epsilon)$ and $\Phi(t, \omega; 0, \omega_0) \approx \delta(t) \cdot \delta(\omega - \omega_0)$ [here ω_ϵ is the frequency of the external field $\mathcal{E}(t)$]. Although, as stated earlier, such a form is mathematically not possible, it can still be used approximately since the "narrowness" in time and in frequency are with respect to different molecular quantities. We can then calculate the integrals with respect to t'', ω_1 for the doorway wavepacket and t, ω for the window wavepacket and obtain the *snapshot limit* of both wavepackets:

$$D_e^{(0)}(xx'; t_0) = \int_{-\infty}^{\infty} d\tau''\, e^{i\omega_\epsilon \tau''} \times \langle x | e^{iH_e(\tau''/2 + t_0)} V_{eg} e^{-iH_g(\tau''/2)} \rho_0 e^{-iH_g(\tau''/2)} V_{ge} e^{iH_e(\tau''/2 - t_0)} | x' \rangle, \tag{3.6}$$

$$W_e^{(0)}(xx'; \omega_0) = \int_{-\infty}^{\infty} d\tau\, e^{i\omega_0 \tau} \langle x | e^{-iH_e(\tau/2)} V_{eg} e^{iH_g \tau} V_{ge} e^{-iH_e(\tau/2)} | x' \rangle. \tag{3.7}$$

The ideal snapshot spectrum is obtained by substituting Eqs. (3.6) and (3.7) in Eq. (3.2).

IV. NUCLEAR WAVEPACKETS IN PUMP–PROBE SPECTROSCOPY

In this section we apply the same formalism to pump–probe spectroscopy, where one measures the absorption of a probe pulse $\mathcal{E}_2(t)$ by a molecule excited by a pump pulse $\mathcal{E}_1(t)$. The pump–probe signal can be written as

$$I_{\mathrm{PP}} = -2\mathrm{Im} \int_{-\infty}^{\infty} \mathcal{E}_2^*(t) \mathcal{P}_2(t)\, dt \tag{4.1}$$

where $\mathcal{P}_2(t)$ is the polarization induced in the sample by the external electric field.

We start by expanding the polarization to first order in the probe amplitude $\mathcal{E}_2^*(t)$:

$$\mathcal{P}_2(t) = \int_{-\infty}^{\infty} d\tau\, \tilde{S}^{(1)}(t,\tau)\mathcal{E}_2(\tau)$$

where $\tilde{S}^{(1)}(t,\tau)$ is the response function linear in the probe [17],

$$\tilde{S}^{(1)}(t,\tau) = i\theta(t-\tau)\langle[\mathcal{P}_2'(t),\mathcal{P}_2'(\tau)]\rangle$$

$\theta(t-\tau)$ is the Heaviside step function and $\mathcal{P}'(t)$ is the polarization operator in the Heisenberg picture, calculated with respect to the Hamiltonian H', which includes the pump field but excludes the probe:

$$\mathcal{P}_2'(t) = \exp\left\{i\int_{-\infty}^{t} H'(\tau)\,d\tau\right\}\mathcal{P}_2'(-\infty)\exp\left\{-i\int_{-\infty}^{t} H'(\tau)\,d\tau\right\}$$

The pump–probe signal can then be written as

$$I_{\mathrm{PP}} = 2\mathrm{Re}\int_{-\infty}^{\infty} dt\int_{-\infty}^{t} d\tau\, \mathcal{E}_2^*(t)\mathcal{E}_2(\tau)\langle[\mathcal{P}_2'(t),\mathcal{P}_2'(\tau)]\rangle \tag{4.2}$$

This formula resembles Eq. (2.6) for the autocorrelation signal. We can further expand $\tilde{S}^{(1)}(t,\tau)$ to second order in the pump field and express the result in terms of the four-point correlation function (2.8) (see Appendix E).

Similar to the correlation measurements discussed in the previous sections, we can define the doorway and window wavepackets and write the signal as their overlap in phase space. The derivation is presented in Appendix E, and we have

$$I_{\mathrm{PP}}(t_0,\omega_0) = \iint dx\; dx'[W_e(xx';\omega_0)D_e(xx';t_0) + W_g(xx';\omega_0)D_g(xx';t_0)] \tag{4.3}$$

where t_0 is the delay between the pump and probe pulses and ω_0 is the carrier frequency of the probe. Upon transforming from the coordinate to the Wigner phase-space representation, we can write (4.3) as

$$I_{PP}(t_0, \omega_0) = \iint dp\ dq[W_e(pq; \omega_0)D_e(pq; t_0) + W_g(pq; \omega_0)D_g(pq; t_0)] \tag{4.4}$$

The wavepackets D_j, W_j, $j = g, e$, can be written in the coordinate representation as

$$D_e(xx'; t_0) = \frac{1}{2\pi} \int\int\int_{-\infty}^{\infty} dt''\ d\tau''\ d\omega_1\ \mathcal{W}_1(t'', \omega_1)e^{i\omega_1\tau''} \times \langle x|e^{iH_e(\tau''/2 - t'' + t_0)}V_{eg}e^{-iH_g(\tau''/2)}\rho_0 e^{-iH_g(\tau''/2)} \cdot V_{ge}e^{iH_e(\tau''/2 + t'' - t_0} \tag{4.5}$$

$$D_g(xx'; t_0) = \frac{1}{2\pi} \int\int\int_{-\infty}^{\infty} dt''\ d\tau''\ d\omega_1\ \mathcal{W}_1(t'', \omega_1)e^{i\omega_1\tau''} \times \langle x|e^{-iH_g(t'' + t_0)}\rho_0 e^{-iH_g(\tau''/2)}V_{ge}e^{iH_e\tau''} \cdot V_{eg}e^{iH_g(-\tau''/2 + t'' - t_0)}|x'\rangle \tag{4.6}$$

$$W_e(xx'; \omega_0) = \frac{1}{2\pi} \int\int\int_{-\infty}^{\infty} dt\ d\tau\ d\omega\ \mathcal{W}_2(t, \omega)e^{i\omega\tau} \times \langle x|e^{-iH_e(\tau/2 - t)}V_{eg}e^{iH_g\tau}V_{ge}e^{-iH_e(\tau/2 + t)}|x'\rangle \tag{4.7}$$

$$W_g(xx'; \omega_0) = \frac{1}{2\pi} \int\int\int_{-\infty}^{\infty} dt\ d\tau\ d\omega\ \mathcal{W}_2(t, \omega)e^{i\omega\tau} \times \langle x|e^{-iH_g(t + \tau/2)}V_{ge}e^{iH_e\tau}V_{eg}e^{iH_g(-\tau/2 + t)}|x'\rangle \tag{4.8}$$

The first term in Eq. (4.3) is reminiscent of Eq. (3.2) for the spontaneous emission spectrum. It represents a doorway wavepacket created by the pump in the excited state, which is then detected by its overlap with a window. The only difference is that the role of the gate in determining the window in SLE is now played by the probe Wigner function $\mathcal{W}_2$. In addition, the pump–probe signal contains a second term that does not show up in fluorescence. This term represents a wavepacket created in the ground state (a "hole") that evolves in time as well and is finally determined by a different window W_g [24]. In the snapshot limit, defined in the preceding section, we have

$$D_e^{(0)}(xx';t_0) = \int_{-\infty}^{\infty} d\tau''\ e^{i\omega_e\tau''} \times \langle x|e^{iH_e(\tau''/2+t_0)}V_{eg}e^{-iH_g(\tau''/2)}\rho_0 e^{-iH_g(\tau''/2)}\cdot V_{ge}e^{iH_e(\tau''/2-t_0)}|x'\rangle$$

$$D_g^{(0)}(xx';t_0) = \int_{-\infty}^{\infty} d\tau''\ e^{i\omega_e\tau''}\langle x|\rho_0 e^{-iH_g(\tau''/2+t_0)}V_{ge}e^{iH_e\tau''}\cdot V_{eg}e^{-iH_g(\tau''/2-t_0)}|x'\rangle$$

$$W_e^{(0)}(xx';\omega_0) = \int_{-\infty}^{\infty} d\tau\ e^{i\omega_0\tau}\langle x|e^{-iH_e(\tau/2)}V_{eg}e^{iH_g\tau}V_{ge}e^{-iH_e(\tau/2)}|x'\rangle$$

$$W_g^{(0)}(xx';\omega_0) = \int_{-\infty}^{\infty} d\tau\ e^{i\omega_0\tau}\langle x|e^{-iH_g(\tau/2)}V_{ge}e^{iH_e\tau}V_{eg}e^{-iH_g(\tau/2)}|x'\rangle$$

V. EXTENSION TO HETERODYNE-DETECTED FOUR-WAVE MIXING

The description of pump–probe signals presented in the preceding section can be immediately generalized to heterodyne-detected transient grating spectroscopy as well as to other four-wave mixing techniques. Heterodyne detection involves mixing the scattered field with an additional heterodyne field $\mathcal{E}_4(t)$. The signal in the $\mathbf{k}_s$ direction can then be written in terms of the polarization $\mathcal{P}_s(t)$ as

$$I_{\mathrm{TG}} = -2\mathrm{Im}\int_{-\infty}^{\infty}\mathcal{E}_4^*(t)\mathcal{P}_s(t)\,dt \tag{5.1}$$

Consider the signal emitted in the direction $\mathbf{k}_s = \mathbf{k}_3 - \mathbf{k}_2 + \mathbf{k}_1$. The polarization $\mathcal{P}_s(t)$ is given by Eq. (E1) except that now the two fields that excite the sample are different. We therefore get

$$\mathcal{P}_s^{(3)}(t) = -i\int_0^{\infty}dt_1\int_0^{\infty}dt_2\int_0^{\infty}dt_3[R_2^{(3)}(t_3,t_2,t_1)+R_3^{(3)}(t_3,t_2,t_1)] \times \mathcal{E}_3(t-t_3)\mathcal{E}_1(t-t_3-t_2)\mathcal{E}_2^*(t-t_3-t_2-t_1)$$
$$-i\int_0^{\infty}dt_1\int_0^{\infty}dt_2\int_0^{\infty}dt_3[R_1^{(3)}(t_3,t_2,t_1)+R_4^{(3)}(t_3,t_2,t_1)] \times \mathcal{E}_3(t-t_3)\mathcal{E}_2^*(t-t_3-t_2)\mathcal{E}_1(t-t_3-t_2-t_1) \tag{5.2}$$

Here the time ordering of the $\mathcal{E}_1$ and $\mathcal{E}_2$ fields can be arbitrary; we only assume that the field $\mathcal{E}_3$ comes after $\mathcal{E}_1$ and $\mathcal{E}_2$ and does not overlap with them. We can then follow the calculations of pump–probe signals in Appendix E and introduce the joint Wigner distribution for the fields $\mathcal{E}_1$ and $\mathcal{E}_2$ and for the field $\mathcal{E}_3$ and $\mathcal{E}_4$:

$$\mathcal{W}_{21}(t,\omega) = \int_{-\infty}^{\infty} \mathcal{E}_2^*(t - \tfrac{1}{2}\tau)\mathcal{E}_1(t + \tfrac{1}{2}\tau)e^{i\omega\tau}\, d\tau$$

$$\mathcal{W}_{43}(t,\omega) = \int_{-\infty}^{\infty} \mathcal{E}_4^*(t - \tfrac{1}{2}\tau)\mathcal{E}_3(t + \tfrac{1}{2}\tau)e^{i\omega\tau}\, d\tau$$

Substituting this into (5.1), we get

$$\begin{aligned} I_{\mathrm{TG}} = \frac{2}{(2\pi)^2}\,\mathrm{Re} \iint_{-\infty}^{\infty} d\omega'\, d\omega'' \int_{-\infty}^{\infty} dt \int_0^{\infty} dt_1 \int_0^{\infty} dt_2 \int_0^{\infty} dt_3 \\ \times [R_2^{(3)}(t_3,t_2,t_1) + R_3^{(3)}(t_3,t_2,t_1) + R_1^{(3)}(t_3,t_2,t_1) + R_4^{(3)}(t_3,t_2,t_1)] \\ \times \mathcal{W}_{43}(t - \tfrac{1}{2}t_3, \omega'')\mathcal{W}_{21}(t - t_3 - t_2 - \tfrac{1}{2}t_1, \omega')e^{-i\omega' t_1}e^{-i\omega'' t_3} \end{aligned} \tag{5.3}$$

The doorway–window picture applies here as well. We can use Eqs. (4.5)–(4.8) provided we replace the pump wavepacket $\mathcal{W}_1$ by $\mathcal{W}_{21}$ and the probe wavepacket $\mathcal{W}_2$ by $\mathcal{W}_{43}$.

APPENDIX A: TIME- AND FREQUENCY-GATED AUTOCORRELATION SIGNALS

Autocorrelation signals may be observed by passing the field through two gating devices, a spectral and a time gate. Each gate has its transmission function (in the time and frequency domain) centered at ω_0 and t_0, respectively. The field passing through each of these gates becomes

$$\mathcal{E}(\omega) = \mathcal{F}_s(\omega;\omega_0)\tilde{\mathcal{E}}(\omega)$$

$$\mathcal{E}(t) = \mathcal{F}_t(t;t_0)\tilde{\mathcal{E}}(t)$$

Here $F_s(\omega;\omega_0)$ and $\mathcal{F}_t(t;t_0)$ are the spectral and temporal transmission functions and $\tilde{\mathcal{E}}$ and $\mathcal{E}$ are the fields before and after passing through the gate, respectively. We shall denote them the bare and the gated signal, and throughout this appendix bare quantities will be denoted by a tilde. Note that the order in which the two gates are applied is important, even though both

devices are linear and independently controlled. From a practical point of view, to attain optimal time and frequency resolution, it is advantageous to apply first the gate with the less ideal transfer function [25]. Below we will consider both configurations.

The measured signal (the total energy received by the detector) is given by Eq. (2.3), except that the field now passes through gating devices prior to its detection. Therefore, the signal becomes a function of both ω_0 and t_0, thus retaining its temporal and spectral information. The *autocorrelation signal* is defined by Eq. (2.4). We will show in Appendix B that within the slowly varying amplitude approximation the measured field is proportional to the polarization induced in the sample by the external electric fields [Eq. (B4)]. We therefore have

$$I_{\text{Auto}}(t_0, \omega_0) = \int_{-\infty}^{\infty} \langle \mathcal{P}_j^*(t) \mathcal{P}_j(t) \rangle \, dt$$

It was shown elsewhere [26] that the gated signal $I_{\text{Auto}}(t_0, \omega_0)$ is given by Eq. (2.5) together with (2.6).

The transmission function is expressed in terms of the Wigner functions for the gates,

$$\mathcal{W}_s(t, \omega) = \int_{-\infty}^{\infty} \mathcal{F}_s^*(\omega - \tfrac{1}{2}\omega') \mathcal{F}_s(\omega + \tfrac{1}{2}\omega') e^{-i\omega' t} \, d\omega'$$

$$\mathcal{W}_t(t, \omega) = \int_{-\infty}^{\infty} \mathcal{F}_t^*(t - \tfrac{1}{2}\tau) \mathcal{F}_t(t + \tfrac{1}{2}\tau) e^{i\omega\tau} \, d\tau$$

If the spectral gate is applied first, we have

$$\Phi_{st}(t', \omega'; t_0, \omega_0) = \int\int_{-\infty}^{\infty} \frac{dt \, d\omega}{2\pi} \mathcal{W}_t(t, \omega; t_0) \mathcal{W}_s(t - t', \omega'; \omega_0) \qquad \text{(A1)}$$

where the subscript st indicates that the signal first passes through the spectral gate and then through the time gate. For the reverse order of the gates, we have

$$\Phi_{ts}(t', \omega'; t_0, \omega_0) = \int\int_{-\infty}^{\infty} \frac{dt \, d\omega}{2\pi} \mathcal{W}_s(t, \omega; \omega_0) \mathcal{W}_t(t', \omega - \omega'; t_0) \qquad \text{(A2)}$$

These two equations can also be written in another form using the definition

of the Wigner function, we then have

$$\Phi_{st}(t', \omega'; t_0, \omega_0) = \int_{-\infty}^{\infty} dt |\mathcal{F}_t(t; t_0)|^2 \mathcal{W}_s(t - t', \omega'; \omega_0) \tag{A3}$$

$$\Phi_{ts}(t', \omega'; t_0, \omega_0) = \int_{-\infty}^{\infty} \frac{d\omega}{2\pi} |\mathcal{F}_s(\omega; \omega_0)|^2 \mathcal{W}_t(t', \omega - \omega';\ t_0) \tag{A4}$$

Assuming specific forms of the time and spectral gates, we get the signal measured in different experimental setups. If the time gate is infinitely short, $\mathcal{F}_t(t; t_0) = \delta(t - t_0)$, we obtain the spectrograms discussed in Ref. [16]. If the signal passes only through the time gate, then the gate acts like the reference pulse in the FROG configuration.

The joint gate function is centered around the frequency ω_0 and the time t_0 and acts as a filter on the bare signal $\tilde{I}$. As an example we shall consider the case when the spectral gate is given by the Fabri–Perot étalon [16] and the time gate is exponential,

$$\mathcal{F}_s(\omega; \omega_0) = \frac{\gamma}{\gamma - i(\omega - \omega_0)} \tag{A5}$$

$$\mathcal{F}_t(t; t_0) = e^{-\Gamma|t - t_0|} \tag{A6}$$

Note that in this case the transmission functions (A5) and (A6) depend on t, t_0 and ω, ω_0 only through the differences $t - t_0$ and $\omega - \omega_0$ and the joint gate function $\Phi_{st}(t', \omega'; t_0, \omega_0)$ only depends on $T \equiv t' - t_0$ and $\Omega \equiv \omega' - \omega_0$. The joint gate function for the gates (A5) and (A6), calculated by (A3), assumes the form

$$\Phi_{st}(T, \Omega) = \begin{cases} \dfrac{e^{-2\Gamma T}}{\Omega^2 + (\Gamma + \gamma)^2} & T > 0 \\ \dfrac{e^{2\Gamma T}}{\Omega^2 + (\Gamma - \gamma)^2} - \dfrac{4\Gamma e^{2\gamma T}}{(\Omega^2 + \Gamma^2 + \gamma^2)^2 - 4\Gamma^2\gamma^2} & \\ \quad \times \left\{ \gamma \cos 2\Omega T - \dfrac{\Omega^2 + \Gamma^2 - \gamma^2}{2\Omega} \sin 2\Omega T \right\} & T < 0 \end{cases} \tag{A7}$$

In the case $\gamma \gg \Gamma$ the above expression simplifies and can be written in the compact form

$$\Phi_{st}(T,\Omega) = \frac{e^{-2\Gamma|T|}}{\Omega^2+\gamma^2} \tag{A8}$$

For the reverse order of gates, when the signal passes first through the time gate and then through the spectral one, we have

$$\Phi_{ts}(T,\Omega) = \frac{\Gamma}{\gamma}\frac{e^{-2(\gamma+\Gamma)|T|}}{[\Omega^2+(\gamma+\Gamma)^2](\Omega^2+\gamma^2)} \times \{[\Omega^2-\gamma(\gamma+\Gamma)]\cos 2\Omega T - (2\gamma+\Gamma)\sin 2\Omega|T|\} \tag{A9}$$

More elaborate gating profiles may be obtained using pulse-shaping techniques [2, 3].

APPENDIX B: THE SIGNAL AND THE OPTICAL POLARIZATION

We relate here the scattered field to the polarization induced in the sample by external fields. The radiated field is the solution of the Maxwell wave equation

$$\nabla\times\nabla\times\underset{\sim}{E}(\mathbf{r},t) + \frac{1}{c^2}\frac{\partial^2}{\partial t^2}\underset{\sim}{E}(\mathbf{r},t) = -\frac{4\pi}{c^2}\frac{\partial^2}{\partial t^2}\underset{\sim}{P}(\mathbf{r},t) \tag{B1}$$

Here $\underset{\sim}{P}(\mathbf{r},t)$ is the analytic polarization, which is defined in terms of the real polarization $\underset{\sim}{P}^{(r)}(\mathbf{r},t)$ in the same way as the analytic signal was defined in terms of the real signal [Eq. (B1) is usually written for the real field and polarization; however, it follows from their definition that the analytic quantifies satisfy the same equation].

When the analytic polarization $\underset{\sim}{P}(\mathbf{r},t)$ is given, the wave equation is linear and inhomogeneous and can be solved exactly in a closed form. The general solution of Eq. B1 is [17]

$$\mathbf{E}(\mathbf{r},t) = \int d\mathbf{r}'\,dt'\,G(\mathbf{r}-\mathbf{r}';t-t')\underset{\sim}{P}(\mathbf{r}',t') \tag{B2}$$

where

$$G(\mathbf{r}' - \mathbf{r}'; t - t') = \frac{1}{2\pi} \int_{-\infty}^{\infty} d\omega \, e^{-i\omega(t-t')} G(\mathbf{r} - \mathbf{r}'; \omega)$$

and

$$G(\mathbf{r}' - \mathbf{r}'; \omega) = \left(\nabla\nabla + \frac{\omega^2}{c} \right) \frac{e^{i(\omega/c)|\mathbf{r}-\mathbf{r}'|}}{|\mathbf{r} - \mathbf{r}'|}$$

We are interested in far-field limit measurements, that is, when the size of the material system is much smaller than its distance from the detector. In this limit, the usual approximation one makes is [27]

$$|\mathbf{r} - \mathbf{r}'| \approx r - r' \cos \theta$$

where θ is the angle between $\mathbf{r}$ (the vector giving the position of the observation point) and $\mathbf{r}'$ (the variable of integration over the volume of the material). In this approximation the Green function $G(\mathbf{r} - \mathbf{r}; \omega)$ becomes

$$G_{je}(\mathbf{r} - \mathbf{r}'; \omega) = \frac{\omega^2}{c^2} \left(\delta_{jl} - \frac{r_j r_l}{r^2} \right) \frac{e^{i(\omega/c)(r - r' \cos\theta)}}{r}$$

We now use this form for the Green function in Eq. (B2), integrating with respect to ω and using the relation

$$\int \omega^2 e^{-i\omega(t-t_0)} \, d\omega = -2\pi \frac{d^2}{dt^2} \delta(t - t_0)$$

We then integrate with respect to t' and obtain

$$\mathcal{E}_j(\mathbf{r}, t) = -\frac{2\pi}{c^2 r} \left(\delta_{jl} - \frac{r_j r_l}{r^2} \right) \int d\mathbf{r}' \, \frac{\partial^2}{\partial t^2} \mathcal{P}_l \left(\mathbf{r}', t - \frac{r - r' \cos\theta}{c} \right) \quad \text{(B3)}$$

Since we are interested in the far-field case, we can approximate in the integrand $r - r' \cos\theta \approx r$, and therefore, integrate over $\mathbf{r}'$ and obtain the following relation between the scattered field and the polarization:

$$\mathcal{E}_j(\mathbf{r},t) = -\frac{2\pi}{c^2 r}\left(\delta_{jl} - \frac{r_j r_l}{r^2}\right)\frac{\partial^2}{\partial t^2}\mathcal{P}_l^{\text{tot}}\left(t - \frac{r}{c}\right)$$

where $\mathcal{P}^{\text{tot}}(t)$ is the total polarization of the material. Although we have obtained a formula that takes into account retardation effects, we will neglect them in what follows. We also invoke the slowly-varying amplitude approximation setting $\ddot{\mathcal{P}}(t) = -\omega^2\mathcal{P}(t)$. Finally, we can write

$$\mathcal{E}_j(\mathbf{r},t) = \frac{2\pi\omega^2}{c^2 r}\left(\delta_{jl} - \frac{r_j r_l}{r^2}\right)\mathcal{P}_l^{\text{tot}}(t) \tag{B4}$$

Assuming that the polarization $\mathcal{P}_l(\mathbf{r}',t)$ has the form of a plane wave along the z direction,

$$\mathcal{P}_l(\mathbf{r}',t) = \mathcal{P}_l(x',y',t)e^{ikz'}$$

we can integrate over z' in (B3) and get

$$\mathcal{E}_j(\mathbf{r},t) = \frac{2\pi\omega^2}{ikc^2 r}\left(\delta_{jl} - \frac{r_j r_l}{r^2}\right)\mathcal{P}_l^{\text{tot}}(t) \tag{B5}$$

where

$$\mathcal{P}_l^{\text{tot}}(t) = \int\int_{-\infty}^{\infty} dx'\,dy'\;\mathcal{P}_l\;(x',y',t)$$

APPENDIX C: FOUR-POINT CORRELATION FUNCTION EXPRESSION FOR FLUORESCENCE SPECTRA

We consider a molecular system interacting with an external electric field and described by the Hamiltonian

$$H = H_0 - VE(\mathbf{r},t) \tag{C1}$$

where H_0 is the electronic and nuclear molecular Hamiltonian and the dipole operator V represents its interaction with the field. Throughout this section $E(\mathbf{r},t)$ denotes the real field. The autocorrelation function of the polarization operators $\langle\tilde{P}(t_1)\tilde{P}(t_2)\rangle$ is expressed in terms of the dipole operator as

$$\langle\tilde{P}(t_1)\tilde{P}(t_2)\rangle = \text{Tr}[V_H(t)V_H(t_1)\rho(-\infty)] \tag{C2}$$

where $V_H(t)$ denotes the dipole operator whose evolution is governed by the Hamiltonian H:

$$V_H(t) = U(t,-\infty)V(-\infty)U^\dagger(t,-\infty) \qquad U(t,t') \equiv \exp\left\{ i \int_t^{t'} H(t)\, dt \right\}$$

The autocorrelation function (C2) is characterized by three intervals of evolution: from $-\infty$ to t_1, from t_1 to t_2, and from t_2 to $-\infty$ (Fig. 4*a*). It is inconvenient to use the finite interval (t_1, t_2), since the corresponding time integrals will have (variable) finite limits. A more practical way to analyze (C2) is to extend the interval (t_1, t_2) to $-\infty$ and factorize the evolution operator $U(t_1, t_2)$ as $U(-\infty, t_2)U^\dagger(-\infty, t_1)$ (Fig. 4(*b*). We then have

$$\begin{aligned}\langle \tilde{P}(t_1)\tilde{P}(t_2)\rangle = \mathrm{Tr}[&U(t_1,-\infty)V(-\infty)U^\dagger(t_1,-\infty) \\ &\times U(t_2,-\infty)V(-\infty)U^\dagger(t_2,-\infty)\rho(-\infty)]\end{aligned}$$

Perturbative expansion with respect to the external electric field yields,

$$\begin{aligned}\langle \tilde{P}(t_1)\tilde{P}(t_2)\rangle = \sum_{j,l,m,i}^{j+l+m+i=n} &\int_0^\infty ds_1 \cdots \int_0^\infty ds_j \int_0^\infty ds_1'' \cdots \\ &\int_0^\infty ds_l'' \int_0^\infty ds_1''' \cdots \int_0^\infty ds_m''' \int_0^\infty ds_1' \cdots \int_0^\infty ds_i' \\ &\times C^{(n)}_{jlmi}(t_1, t_2; s_1, \ldots, s_j, s_1'', \ldots, s_l'', s_1''', \ldots, s_m''', s_1', \ldots, s_i') \\ &\times E(\mathbf{r}, t_2 - s_j - \cdots - s_1) \cdots E(\mathbf{r}, t_2 - s_j) \\ &\times E(\mathbf{r}, t_2 - s_m''' - \cdots - s_1''') \cdots E(\mathbf{r}, t_2 - s_m''') \\ &\times E(\mathbf{r}, t_1 - s_l'' - \cdots - s_1'') \cdots E(\mathbf{r}, t_1 - s_l'') \\ &\times E(\mathbf{r}, t_1 - s_i' - \cdots - s_1') \cdots E(\mathbf{r}, t_1 - s_i') \qquad \text{(C3)}\end{aligned}$$

with

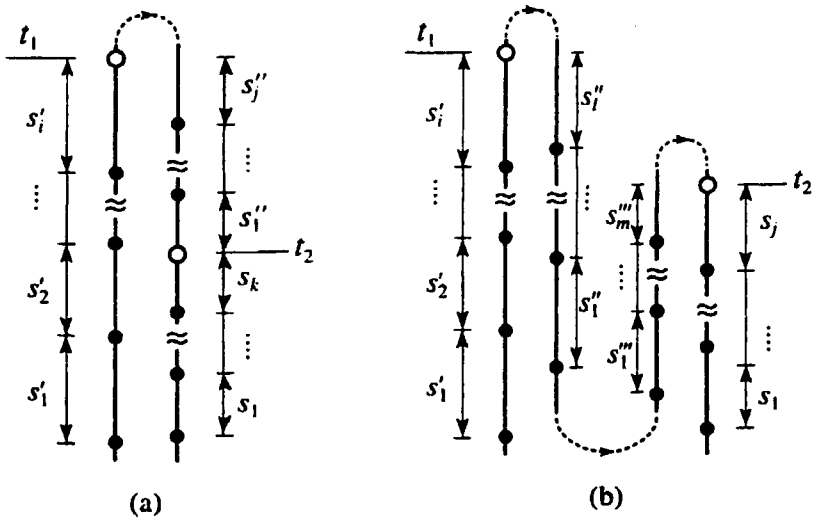

Figure 4. Two ways to describe the time-evolution of the dipole operators: single (*a*) and double (*b*) Liouville space diagrams.

$$
\begin{aligned}
C^{(n)}_{jlmi}(t_1, t_2; s_1, \ldots, s_j, s_1'', \ldots, s_l'', s_1''', \ldots, s_m''', s_1', \ldots, s_i') \\
&= \langle V(t_1 - s_j - \cdots - s_1) \cdots V(t_1 - s_j) V(t_1) \\
&\quad \times V(t_2 - s_l'' - \cdots - s_1'') \cdots V(t_2 - s_l'') \\
&\quad \times V(t_2 - s_m''' - \cdots - s_1''') \cdots V(t_2 - s_m''') V(t_2) \\
&\quad \times V(t_2 - s_i' - \cdots - s_1') \cdots V(t_2 - s_i') \rangle
\end{aligned}
\tag{C4}
$$

Here $V(t)$ is the dipole moment given by Eq. (2.9).

For $n = 2$ the subscripts j, l, m, i take the values 0, 1, 2 (so that their sum is at most 2), and the result is expressed in terms of the four-point correlation functions:

$$
\begin{aligned}
\langle \tilde{P}(t_1) \tilde{P}(t_2) \rangle = \int_0^\infty ds_1 \int_0^\infty ds_2 \{ & C^{(2)}_{2000}(t_1, t_2; s_1, s_2) E(\mathbf{r}, t_1 - s_1 - s_2) E(\mathbf{r}, t_1 - s_2) \\
& + C^{(2)}_{0020}(t_1, t_2; s_1, s_2) E(\mathbf{r}, t_2 - s_1 - s_2) E(\mathbf{r}, t_2 - s_2) \\
& + C^{(2)}_{1100}(t_1, t_2; s_1, s_2) E(\mathbf{r}, t_1 - s_1) E(\mathbf{r}, t_1 - s_2) \\
& + C^{(2)}_{1010}(t_1, t_2; s_1, s_2) E(\mathbf{r}, t_1 - s_1) E(\mathbf{r}, t_2 - s_2) \\
& + C^{(2)}_{1001}(t_1, t_2; s_1, s_2) E(\mathbf{r}, t_1 - s_1) E(\mathbf{r}, t_2 - s_2) \\
& + C^{(2)}_{0011}(t_1, t_2; s_1, s_2) E(\mathbf{r}, t_2 - s_2) E(\mathbf{r}, t_2 - s_2 - s_1) \} + \text{c.c.}
\end{aligned}
\tag{C5}
$$

where

$$C^{(2)}_{2000}(t_1,t_2;s_1,s_2) = F^{(4)}(t_1 - s_1 - s_2, t_1 - s_2, t_1, t_2)$$
$$C^{(2)}_{0020}(t_1,t_2;s_1,s_2) = F^{(4)}(t_1, t_2 - s_1 - s_2, t_2 - s_2, t_2)$$
$$C^{(2)}_{1100}(t_1,t_2;s_1,s_2) = F^{(4)}(t_1 - s_1, t_1, t_1 - s_2, t_2)$$
$$C^{(2)}_{1010}(t_1,t_2;s_1,s_2) = F^{(4)}(t_1 - s_1, t_1, t_2 - s_2, t_2)$$
$$C^{(2)}_{1001}(t_1,t_2;s_1,s_2) = F^{(4)}(t_1 - s_1, t_1, t_2, t_2 - s_2)$$
$$C^{(2)}_{0011}(t_1,t_2;s_1,s_2) = F^{(4)}(t_1, t_2 - s_1, t_2 - s_2, t_2)$$

We now consider a two-level system and invoke the rotating-wave approximation, in which we neglect highly oscillatory terms. We can now calculate the evolution operator $U_0(t,t')$ explicitly, using the Hamiltonian of the ground and excited states of the two-level system. If ω is close to the transition frequency of the two-level system, then the only term that will not contain highly-oscillating factors $e^{i(\omega+\omega_{eg})t}$ is the term with $C^{(2)}_{1001}$. Keeping this term only, we get

$$\langle \tilde{P}(t_1)\tilde{P}(t_2)\rangle = \int_0^\infty ds_1 \int_0^\infty ds_2 F^{(4)}(t_1 - s_1, t_1, t_2, t_2 - s_2) \times E(\mathbf{r}, t_1 - s_1)E(\mathbf{r}, t_2 - s_2) \tag{C6}$$

This formula can be easily rewritten for the analytic field and polarization. Substitution into Eq. (2.6) finally results in Eq. (2.7).

APPENDIX D: PHASE-SPACE DOORWAY–WINDOW WAVEPACKETS FOR FLUORESCENCE

We now derive the expression for the fluorescence signal in terms of the doorway and window wavepackets instead of the four-point correlation function. We start with Eq. (3.1) and write the four-point correlation function $F^{(4)}$ explicitly as the trace with respect to the equilibrium density matrix. We then use the cyclic invariance of the trace and obtain

$$F^{(4)}(t - \tau' - \tfrac{1}{2}\tau'', t - \tfrac{1}{2}\tau, t + \tfrac{1}{2}\tau, t - \tau' + \tfrac{1}{2}\tau'') = \mathrm{Tr}[V(t - \tfrac{1}{2}\tau)V(t + \tfrac{1}{2}\tau)V(t - \tau' + \tfrac{1}{2}\tau'')V(t - \tau' - \tfrac{1}{2}\tau'')] \tag{D1}$$

We now write the equilibrium density matrix in the coordinate represen-

tation and insert in (D1) the unity operator $\int dx'|x'\rangle\langle x'|$. We then have

$$F^{(4)}(t-\tau'-\tfrac{1}{2}\tau'', t-\tfrac{1}{2}\tau, t+\tfrac{1}{2}\tau, t-\tau'+\tfrac{1}{2}\tau'')$$
$$= \int\int dx\ dx'\ \langle x|V(t-\tfrac{1}{2}\tau)V(t+\tfrac{1}{2}\tau)|x'\rangle$$
$$\times \langle x'|V(t-\tau'+\tfrac{1}{2}\tau'')\rho_0 V(t-\tau'-\tfrac{1}{2}\tau'')|x\rangle \qquad \text{(D2)}$$

We assume that the external field is peaked at the time $-t_0$ and the temporal gate at the time $t = 0$. Changing in the doorway wavepacket the variable $t'' = t + t_0 - \tau'$, we can rewrite equation (D2) as

$$F^{(4)}(t-\tau'-\tfrac{1}{2}\tau'', t-\tfrac{1}{2}\tau, t+\tfrac{1}{2}\tau, t-\tau'+\tfrac{1}{2}\tau'')$$
$$= \int\int dx\ dx'\ \rho_W(xx';t,\tau)\rho_D(xx';t'',\tau'') \qquad \text{(D3)}$$

where

$$\rho_D(xx';t'',\tau'') = \langle x|V(t''-t_0+\tfrac{1}{2}\tau'')\rho_0 V(t''-t_0-\tfrac{1}{2}\tau'')|x'\rangle,$$

is the doorway wavepacket created by the external field, and

$$\rho_W(xx';t,\tau) = \langle x|V(t-\tfrac{1}{2}\tau)V(t+\tfrac{1}{2}\tau)|x'\rangle,$$

is the window wavepacket. The response function is then calculated by the overlap of the window wavepacket with the doorway wavepacket propagated for the time t_0. These formulas can be rewritten in the Heisenberg picture,

$$\rho_D(x,x';t'',\tau'')$$
$$= \langle x|e^{iH_e(\tau''/2-t''+t_0)}V_{eg}e^{-iH_g(\tau''/2)}\rho_0 e^{-iH_g(\tau''/2)}V_{ge}e^{iH_e(\tau''/2+t''-t_0)}|x'\rangle$$
$$\rho_W(x,x';t,\tau)$$
$$= \langle x|e^{-iH_e(\tau/2-t)}V_{eg}e^{iH_g(\tau/2)}e^{iH_g(\tau/2)}V_{ge}e^{-iH_e(\tau/2+t)}|x'\rangle$$

We now return to the expression for the gate signal (2.5) and substitute the bare signal (3.1) with the four-point correlation function $F^{(4)}$ replaced with the doorway and window wavepackets as in (D3). We then separate the four time integrals into two groups: the integrals with respect to t'' and τ'' for the doorway wavepacket and with respect to t and τ for the window wavepacket. We can also change all limits of integration to infinity; this is

possible since we assumed that the Wigner function of the incoming field $\mathcal{W}_{\mathcal{E}}$ and the gate function Φ are well separated in time. We then obtain Eqs. (3.2)–(3.4).

APPENDIX E: DOORWAY–WINDOW PHASE-SPACE WAVEPACKETS FOR PUMP–PROBE SIGNALS

We shall calculate here the pump–probe signal (4.1) using the doorway window wavepackets representation. The polarization $\mathcal{P}_2(t)$ to third order in the external field is given in Ref. 17 and is shown to be expressed in terms of the four-point correlation function (2.8):

$$\begin{aligned}\mathcal{P}_2^{(3)}(t) = -i \int_0^\infty dt_1 \int_0^\infty dt_2 \int_0^\infty dt_3\, [R_2^{(3)}(t_3,t_2,t_1) + R_3^{(3)}(t_3,t_2,t_1)] \\ \times \mathcal{E}_2(t-t_3)\mathcal{E}_1(t-t_3-t_2)\mathcal{E}_1^*(t-t_3-t_2-t_1) \\ - i \int_0^\infty dt_1 \int_0^\infty dt_2 \int_0^\infty dt_3 [R_1^{(3)}(t_3,t_2,t_1) + R_4^{(3)}(t_3,t_2,t_1)] \\ \times \mathcal{E}_2(t-t_3)\mathcal{E}_1^*(t-t_3-t_2)\mathcal{E}_1(t-t_3-t_2-t_1) \qquad \text{(E1)}\end{aligned}$$

where

$$\begin{aligned}R_1^{(3)}(t_3,t_2,t_1) &= F^{(4)}(t-t_3-t_2-t_1, t, t-t_3, t-t_3-t_2) \\ R_2^{(3)}(t_3,t_2,t_1) &= F^{(4)}(t-t_3-t_2, t, t-t_3, t-t_3-t_2-t_1) \\ R_3^{(3)}(t_3,t_2,t_1) &= F^{(4)}(t-t_3, t, t-t_3-t_2, t-t_3-t_2-t_1) \\ R_4^{(3)}(t_3,t_2,t_1) &= F^{(4)}(t-t_3-t_2-t_1, t-t_3-t_2, t-t_3, t)\end{aligned}$$

Substituting this into (4.1) and introducing the Wigner representation for the pump and the probe fields as was done for the fluorescence, we get

$$\begin{aligned}I_{\mathrm{PP}} = \frac{2}{(2\pi)} \mathrm{Re} \iint_{-\infty}^{\infty} d\omega'\, d\omega'' \int_{-\infty}^{\infty} dt \int_0^\infty dt_1 \int_0^\infty dt_2 \int_0^\infty dt_3 \\ \times [R_2^{(3)}(t_3,t_2,t_1) + R_3^{(3)}(t_3,t_2,t_1) + R_1^{(3)}(t_3,t_2,t_1) + R_4^{(3)}(t_3,t_2,t_1)] \\ \times \mathcal{W}_2(t-\tfrac{1}{2}t_3, \omega'')\mathcal{W}_1(t-t_3-t_2-\tfrac{1}{2}t_1, \omega') e^{-i\omega' t_1} e^{-i\omega'' t_3} \qquad \text{(E2)}\end{aligned}$$

Similar to the fluoresence discussed in Appendix D, we can define doorway and window wavepackets and write the signal as their phase-space overlap. Assuming that the delay time between the probe and the pump pulses is t_0, we obtain Eqs. (4.5)–(4.8).

Acknowledgments

The support of the National Science Foundation and the Air Force Office of Scientific Research is gratefully acknowledged.

References

1. D. J. Tannor and S. A. Rice, *J. Phys. Chem.* **83,** 5013 (1985).
2. A. M. Weiner, *Prog. Quantum Electron.* **19,** 161 (1995).
3. J. T. Fourkas, L. Dhar, K. A. Nelson, and R. Trebino, *J. Opt. Soc. Am. B* **12,** 155 (1995).
4. N. F. Scherer, L. D. Zeigler, and G. R. Fleming, *J. Chem. Phys.* **96,** 5544 (1992).
5. W. S. Warren, H. Rabitz, and M. Dahleh, *Science* **259,** 1581 (1993).
6. B. Kohler, J. L. Krause, F. Raksi, C. Rose-Petruck, R. M. Whitnell, K. R. Wilson, V. V. Yakovlev, Y. Yan, and S. Mukamel, *J. Phys. Chem.* **97,** 12602 (1993).
7. B. Kohler, V. V. Yakovlev, J. Che, J. L. Krause, M. Messina, and K. R. Wilson, *Phys. Rev. Lett* **74,** 3360 (1995).
8. W. Koenig, H. K. Dunn, and L. Y. Lacy, *J. Acoust. Soc. Am.* **18,** 19 (1946).
9. D. J. Kane and R. Trebino, *IEEE J. Quantum Electron.* **29,** 2 (1993).
10. R. Trebino and D. J. Kane, *J. Opt. Soc. Am. A* **10,** 1101 (1993).
11. J. Paye, *IEEE J. Quantum Electron.* **28,** 2262 (1992).
12. J. Paye, in *Ultrafast Phenomena*, Vol. 9, P. F. Barbara, W. H. Knox, G. A. Mourou, and A. H. Zewail, Eds., Springer-Verlag, New York 1994.
13. L. Cohen, *Proc. IEEE* **77,** 941 (1989).
14. L. Mandel and E. Wolf, Eds., *Selected Papers on Coherence and Fluctuations of Light, with Bibliography*, Dover, 1970.
15. M. G. Raymer, M. Beck, and D. T. Smithey, *Phys. Rev. Lett.* **70,** 1244 (1993).
16. H. Stolz, *Time-Resolved Light Scattering from Excitons*, Springer, Verlag, Berlin; New York 1994.
17. S. Mukamel, *Principles of Nonlinear Optical Spectroscopy*, Oxford University Press, New York 1995.
18. H. M. Nussenzweig, *Introduction to Quantum Optics*, Gordon & Breach, London; New York 1973.
19. E. T. J. Nibbering, D. A. Wiersma, and K. Duppen, *Phys. Rev. Lett.* **66,** 2464 (1991).
20. D. C. Arnett, P. Vöhringer, R. A. Westervelt, M. J. Feldstein, and N. F. Scherer, in *Ultrafast Phenomena*, Vol. 9, P. F. Barbara, W. H. Knox, G. A. Mourou, and A. H. Zewail, Eds., Springer-Verlag, Berlin 1994.
21. W. P. de Boeij, M. S. Pshenichnikov, and D. A. Wiersma, *Chem. Phys. Lett.* **238,** 1 (1995).
22. P. Vöhringer, D. C. Arnett, T.-S. Yang, and N. F. Scherer, *Chem. Phys. Lett.* **237,** 387 (1995).
23. S. Mukamel, *Adv. Chem. Phys.* **70** (Part I), 165 (1988).

24. Y. J. Yan and S. Mukamel, *Phys. Rev. A* **41,** 6485 (1990).
25. V. Wong and I. A. Walmsley, *J. Opt. Soc. Am. B* **12,** 1491 (1995).
26. S. Mukamel, C. Ciordas-Ciurdariu, and V. Khidekel, *IEEE J. Quantum Electron.*, **32,** 1278 (1996).
27. J. D. Jackson, *Classical Electrodynamics*, Wiley, New York, 1975.

GENERAL DISCUSSION ON LASER CONTROL OF CHEMICAL REACTIONS

Chairman: M. Quack

V. Engel: Prof. Manz, I want to come back to the question of dissipation. We learned from the talk of Prof. Fleming that coherences persist for a while in a liquid surrounding, but not too long. The control schemes we heard about rely on quantum interference or coherence. I would like to know: What are the perspectives of applying the control schemes to chemical reactions in a liquid?

J. Manz: Prof. V. Engel's question points to the virtues of using (i) ultrashort laser pulses for controlling chemical reactions, in comparison with (ii) continuous-wave lasers. Compare, for example, the strategies of (i) Tannor et al. [1], Rabitz [2], Combariza et al. [3] (see also Korolkov et al., "Theory of Laser Control of Vibrational Transitions and Chemical Reactions by Ultrashort Infrared Laser Pulses," this volume) versus (ii) the strategies of Brumer and Shapiro [4] or Letokhov [5] and others [6]. See the review by S. A. Rice (this volume). Intuitively, one may assume that the advantage of using ultrashort laser pulses should be that they can be faster and, therefore, "beat" competing dissipative processes such as intramolecular vibrational redistribution (IVR). This argument is supported, certainly, by the observation of relatively long coherence lifetimes of reactive wavepackets even in the condensed phase, as has been demonstrated beautifully by G. R. Fleming et al. ("Femtosecond Chemical Dynamics in Condensed Phases," this volume) and A. H. Zewail [7]. However, this advantage may be valid only for rather strong laser fields, because, otherwise, for weak laser fields, there is a theorem by Brumer and Shapiro saying that time-dependent and time-independent fields will achieve equivalent molecular transitions [8].

1. D. J. Tannor and S. A. Rice, *J. Chem. Phys.* **83,** 5013 (1985); D. J. Tannor, R. Kosloff, and S. A. Rice, *J. Chem. Phys.* **85,** 5805 (1986); D. J. Tannor and S. A. Rice, *Adv. Chem. Phys.* **70,** 441 (1988).

2. S. Shi, A. Woody, and H. Rabitz, *J. Chem. Phys.* **88,** 6870 (1988); W. S. Warren, H. Rabitz, and M. Dahleh, *Science* **259,** 1581 (1993); W. Jakubetz, J. Manz, and H.-J. Schreiber, *Chem. Phys. Lett.* **165,** 100 (1990); W. Jakubetz, E. Kades, and J. Manz, *J. Phys. Chem.* **97,** 12609 (1993).

3. J. E. Combariza, B. Just, J. Manz, and G. K. Paramonov, *J. Chem. Phys.* **95,** 10355 (1991).
4. M. Shapiro and P. Brumer, *J. Chem. Phys.* **84,** 4103 (1986); P. Brumer and M. Shapiro, *Acc. Chem. Res.* **22,** 407 (1994).
5. V. Letokhov, *Science* **180,** 451 (1973).
6. E. Segev and M. Shapiro, *J. Chem. Phys.* **77,** 5604 (1982); V. Engel and R. Schinke, *J. Chem. Phys.* **88,** 6831 (1988); D. G. Imre and J. Zhang, *J. Chem. Phys.* **89,** 139 (1989); M. D. Likar, J. E. Baggott, A. Sinha, T. M. Ticich, R. L. Vander Wal, and F. F. Crim, *J. Chem. Soc. Faraday Trans. II* **84,** 1483 (1988); F. F. Crim, *Science* **249,** 1387 (1990).
7. A. H. Zewail, in *Femtosecond Chemistry*, J. Manz and L. Wöste, Eds., Verlag Chemie, Weinheim, 1995, p. 15; R. Zadoyan, Z. Li, P. Ashjian, C. C. Martens, and V. A. Apkarian, *Chem. Phys. Lett.* **218,** 504 (1994).
8. M. Shapiro and P. Brumer, *J. Chem. Phys.* **84,** 540 (1985).

M. Shapiro: In relation to the problem discussed by Profs. Engel and Manz, I should point out that, if there are fast dephasings, one definitely would have to use fast pulses. Graham Fleming's data suggest, however, that coherences persist for much longer times than anticipated in the past. In order to overcome decoherence, we can consider adiabatic passage techniques (cf., e.g., Bergmann, Reuss, van Linden van der Heuvel, and Neusser) whose advantage is that you can completely empty the ground state, irrespective of the exact pulse shape, provided that the area under the pulse $[\int dt\mathcal{E}(t)\mu]$ exceeds the limit imposed by the adiabatic condition.

L. Wöste: Prof. Manz, when you shape potential-energy curves or surfaces with high-intensity IR laser fields, don't you believe that these field strengths can also induce electronic transitions leading to entirely different states and potential-energy surfaces, so that the proposed shaping process loses relevance?

M. V. Korolkov, J. Manz, and G. K. Paramonov:* We are fully aware of the danger of using exceedingly intense IR picosecond/femtosecond laser pulses for control of molecular vibrations or reactions. As a rule derived from laser interactions with atoms, the intensities should be below the Keldish limit [1],

$$I_{\text{Keldish}} = \frac{\epsilon_0 c}{2}\left(\frac{4\pi\epsilon_0}{e^3}\right)^2 \frac{E_S^4}{16Z^2} \tag{1}$$

*Comment presented by J. Manz.

$$I_{\text{Keldish}} = \frac{4 \times 10^9 (E_s)^4}{Z^2} \text{ W/cm}^2 \tag{2}$$

where E_S is the ionization potential in electron-volts. Otherwise the laser may ionize the atoms, yielding a large displacement r_0 in the presence of an electric field with amplitude $\mathcal{E}_0$ and carrier frequency ω [2]:

$$r_0 = \frac{e\mathcal{E}_0}{m\omega^2} \tag{3}$$

$$\frac{r_0}{a_0} = (2.57 \times 10^{-12})\, I^{1/2} \times \lambda^2$$

$$= \frac{257\, I^{1/2}}{(1/\tilde{\lambda})^2} \tag{4}$$

where I is in watts per square centimeters, λ is in nanometers, and $\tilde{\lambda}$ is in reciprocal centimeters. We wish to point out, however, that, to the best of our knowledge, there are so far no systematic investigations of similar Keldish-type limits for molecules. We have carried out exploratory test calculations for a model system that indicate that even stronger intensities may not be sufficient for ionization by ultrashort infrared laser pulses (see Fig. 1).

In any case, one should always try to keep the laser intensities, specifically the amplitudes

$$I_0 = \epsilon_0 c \mathcal{E}_0^2 \tag{5}$$

or the corresponding amplitudes of the laser field strength $\mathcal{E}_0$ as small as possible. There are several ways (i), (ii) or optimal conditions (iii), (iv), (v) for this purpose:

(i) Prolongation of the pulse duration.

(ii) Separation of a single IR femtosecond/picosecond laser pulse into a series of IR femtosecond/picosecond pulses [3].

(iii) Applications to systems with rather strong variations of the dipole function $\mu(q)$ along the vibrational or reaction coordinate (q). Note that the semiclassical molecule–laser interaction operator is

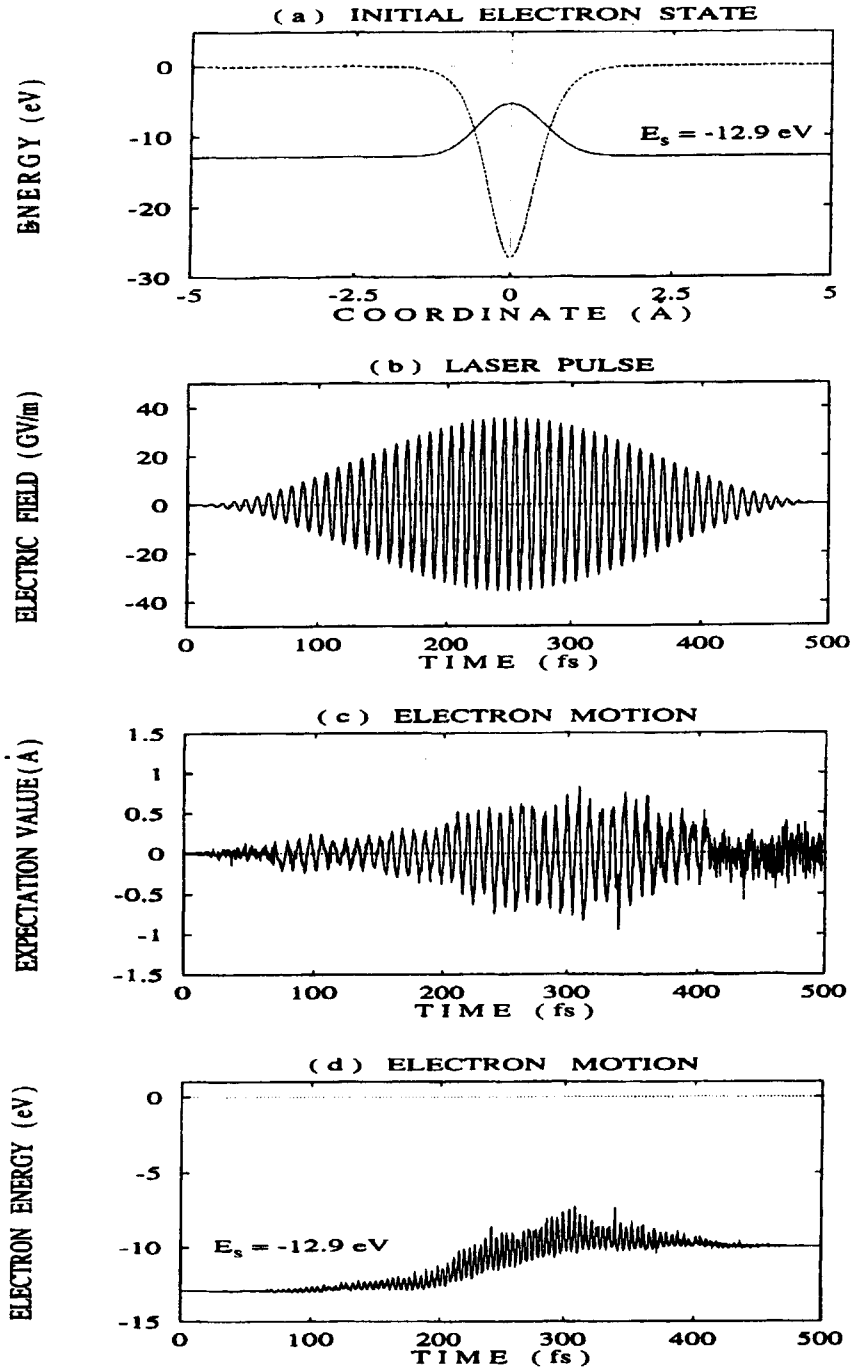

Figure 1. Testing the Keldish limit [1, 2] to ionization by intense infrared femtosecond/picosecond laser pulses used for control of chemical reactions [3, 4]. (*a*) Electronic ground state embedded in a typical model potential curve with the ionization potential E_S = 12.9 eV. (*b*) Intense ($\mathcal{E}_0$ = 35.5 GV/m^{-1}, $I_0 = 3.3 \times 10^{14}$ W/cm^2), ultrashort (t_p = 0.5 ps), infrared ($1/\lambda$ = 3784 cm^{-1}) laser pulse. (*c*) Expectation value for the position of the electron, which is driven by the laser field shown in panel (*b*) [compare with r_0 = 122 Å, Eq. (3)]. (*d*) Electron energy. These model calculations demonstrate that even very intense ($I > I_{\text{Keldish}}$) ultrashort IR laser pulses may not cause ionization; that is, the simple estimates (1)–(4) [1, 2] are not applicable.

$$H(t) = -\mu(q) \cdot \mathcal{E}(t) \tag{6}$$

that is, large variations of $\mu(q)$ may allow use of rather small values of field amplitudes $\mathcal{E}_0$ and, therefore, intensities [cf. Eq. (5)].

(iv) Applications to vibrational transitions between close (say Δv = 1, 2, 3, ..., not 10, 20, 30, ...) vibrational levels.

(v) For applications to isomerizations, items (iii) and (iv) imply that the reaction should proceed across rather shallow barriers of the potential energy surface, and the reactants and products should have rather different (e.g., with opposite signs) dipole moments. (See also Korolkov et al., "Theory of Laser Control of Vibrational Transitions and Chemical Reactions by Ultrashort Infrared Laser Pulses," this volume; supported by DFG.)

1. L. V. Keldish, *Sov. Phys. JETP* **20,** 1307 (1965); S. Augst, D. D. Meyerhofer, D. Strickland, and S. L. Chin, *J. Opt. Soc. Am. B* **8,** 858 (1991); P. Dietrich and P. B. Corkum, *J. Chem. Phys.* **97,** 3187 (1992).
2. A. D. Bandrauk, in *Femtosecond Chemistry*, J. Manz and L. Wöste, Eds., Verlag Chemie, Weinheim, 1995, p. 261.
3. J. E. Combariza, B. Just, J. Manz, and G. K. Paramonov, *J. Chem. Phys.* **95,** 10351 (1991); B. Just, J. Manz, and G. K. Paramonov, *Chem. Phys. Lett.* **193,** 429 (1992).

M. Quack: Somewhat related to the very nice isomerization scheme used by Dohle and co-workers [1], I would like to make a more general comment.

In connection to "control" in dynamics I would like to take here a general point of view in terms of symmetries (see Scheme 1): We would start with control of some symmetries in an initial state and follow their *time dependence*. This can be used as a test of fundamental symmetries, such as parity, P, time reversal symmetry, T, CP, and CPT, or else we can use the procedure to discover and analyze certain *approximate* symmetries of the molecular dynamics such as nuclear spin symmetry species [2], or certain structural vibrational, rotational symmetries [3].

I would like to draw attention here to some work on chiral molecules, which allows very fundamental tests of symmetries in physics and chemistry. The experiment outlined in Scheme 2 [4] allows us to generate, by laser control, states of well-defined parity in molecules, which are ordinarily left handed (L) or right handed (R) chiral in their ground states. By watching the time evolution of parity, one can test for parity violation and I have discussed in detail [4–6] how parity violating potentials ΔE_{pv} might be measured, even if as

Control of symmetry of initial state

↓

Time dependence of symmetry properties?

↓

Test of fundamental symmetries in nature (such as P, T, CP, CPT)

or

Test of *approximate* symmetries of dynamics

Scheme 1. Control of symmetries in dynamics.

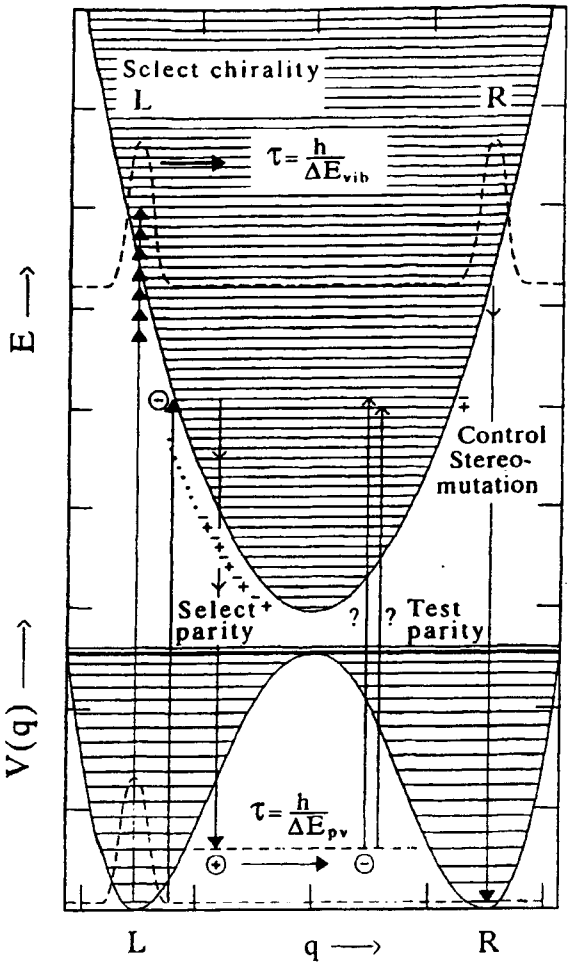

Scheme 2. Control of parity and chirality in the scheme of Ref. 4.

small as 10^{-14} J/mol. Time scales corresponding to such symmetry violation are hours to days. On the other hand, one can also generate a very short-lived time-dependent chiral *excited* state, even if the potential has a minimum at an achiral geometry. If the excited-state potential is harmonic, for example, one may derive interesting results on chirality in relation to harmonic oscillator dynamics [7]. This includes femtosecond evolution of chirality and control of stereomutation in chiral molecules [7].

On the most fundamental level, we have shown how this experimental scheme might be used for a fundamental test of CPT symmetry violation [8]. While still somewhat hypothetical, at present, this would constitute the most sensitive currently proposed test on CPT symmetry. The sensitivity expressed as a baryon mass difference Δm between particles and antiparticles (with mass m) would be of the order of $\Delta m/m \simeq 10^{-30}$ [8]. The best currently *proposed* other experiment is on antihydrogen spectroscopy at CERN (not yet carried out) with $\Delta m/m \simeq 10^{-18}$, and the best **existing** result for the proton–antiproton pair is $\Delta m/m \leq 10^{-9}$ [9].

Relating to the introductory comments by Prof. Prigogine on irreversibility on Tuesday, one might consider time reversal symmetry violation and indeed CPT symmetry violation as a more fundamental approach to this problem. One could then envisage that the second law is not just a de facto violation of time reversal symmetry but a de lege violation in the terminology of Refs. 5 and 6. Figure 1 shows the entropy evolution of CF_2HCl on the femtosecond time scale, showing relaxation toward maximum entropy. With time reversal symmetry, the time reversed dynamic state would return to zero entropy after the appropriate time. This is the current status of experimental knowledge. However, one might envisage that on long time scales for complex systems time reversal symmetry may not apply and entropy stays near the maximum, as drawn roughly as a second option into the figure.

1. M. Dohle, J. Manz, and G. K. Paramonov, *Ber. Bunsenges. Physik. Chem.* **99,** 478 (1995).

2. M. Quack, *Mol. Phys.* **34,** 477 (1977).

3. A. Beil, D. Luckhaus, R. Marquardt, and M. Quack, *J. Chem. Soc. Faraday Discuss.* **99,** 49 (1994); M. Quack, *J. Mol. Struct.* **347,** 245 (1995).

4. M. Quack, *Chem. Phys. Lett.* **132,** 147 (1986).

5. M. Quack, *Angew. Chemie* **101,** 588 (1989); *Angew. Chemie Int. Ed. Engl.* **28,** 571 (1989).

6. M. Quack, in *Femtosecond Chemistry*, J. Manz and L. Wöste, Eds., Verlag Chemie, Weinheim, 1995, Chapter 27. p. 781.

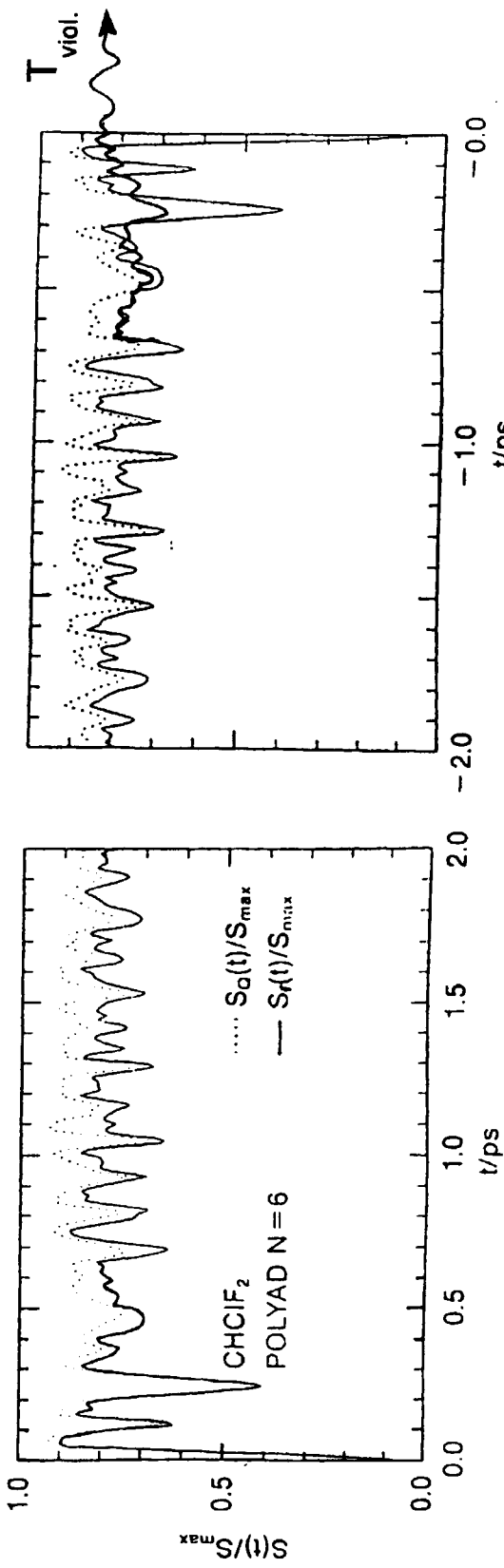

Figure 1. Time-dependent entropy for the three strongly coupled CH stretching and bending vibrations in CF_2HCl [6].

7. R. Marquardt and M. Quack, *J. Chem. Phys.* **90,** 6320 (1989); *J. Phys. Chem.* **98,** 3486 (1994); *Z. Phys. D* **36,** 229 (1996).
8. M. Quack, *Verhand. DPG VI* **28,** 244 (1993); *Chem. Phys. Lett.* **231,** 421 (1994).
9. G. Gabrielse, D. Phillips, W. Quint, H. Kalinowsky, G. Rouleau, and W. Jhe, *Phys. Rev. Lett.* **74,** 3544 (1995); J. Groebner, H. Kalinowsky, D. Phillips, W. Quint, and G. Gabrielse, *Verhand. DPG VI* **28,** 315 (1993).

M. E. Kellman: The idea by Prof. Quack of using molecular experiments to test fundamental symmetries is very interesting. In connection with the Na_3 pseudorotation experiments we heard about yesterday, have you considered testing permutation symmetry of identical particles, that is, the Pauli principle and nuclear spin statistics?

M. Quack: The violation of the principle of nuclear spin symmetry conservation [1] could be seen in a similar scheme as I discussed for parity, but, in contrast to parity violation, it can also be seen by more standard spectroscopic techniques (and has been seen repeatedly). On the other hand, one might also look for violations of the Pauli principle, which in fact we have done [2]. However, it seems unlikely to find such a violation (and nothing of that kind has ever been found), although in principle one must allow even for such a phenomenon.

1. M. Quack, *Mol. Phys.* **34,** 477 (1977).
2. M. Quack, *J. Mol. Struct.* **292,** 171 (1993); and unpublished results.

M. S. Child: I would like to ask Prof. Quack to what extent tunnelling between the two enantiomers might affect these conclusions?

M. Quack: Tunneling will be completely suppressed if $\Delta E_{pv} \gg \Delta E_{tun}$. Even if that is not the case, if ΔE_{pv} is negligible, tunneling may be exceedingly slow, as was already discussed by Hund in 1927 (see Refs. 1 and 2 and references cited therein).

1. M. Quack, *Angew. Chemie* **101,** 588 (1989); *Angew. Chemie Int. Ed. Engl.* **28,** 571 (1998).
2. M. Quack, in *Femtosecond Chemistry*, J. Manz and L. Wöste, Eds., Verlag Chemie, Weinheim, 1995, Chapter 27, p. 781; R. Marquardt and M. Quack, *Z. Phys. D* **36,** 229 (1996).

J. Manz: Prof. M. Quack has just presented to us a fascinating strategy for laser control of chemical enantiomers with different parities [1].

A complementary approach has been suggested earlier by Brumer and Shapiro, based on their general strategy of laser control [2]. I would like to ask Prof. M. Shapiro whether he could comment on his approach in comparison with that of M. Quack.

1. M. Quack, in *Femtosecond Chemistry*, J. Manz and L. Wöste, Eds., Verlag Chemie,

Weinheim, 1995, Chapter 27, p. 781, R. Marquardt and M. Quack, *Z. Phys. D* **36,** 229 (1996).

2. M. Shapiro and P. Brumer, *J. Chem. Phys.* **95,** 8658 (1991).

M. Shapiro: Our approach [M. Shapiro and P. Brumer, "Controlled Photon Induced Symmetry Breaking: Chiral Molecular Products from Achiral Precursors" *J. Chem. Phys.* **95,** 8658 (1991)], differs from that of Quack in that we show how to *generate* chirality (from achiral precursors).

T. Kobayashi: I would like to make the comment that an interesting application of wavepacket control [1] is phonon squeezing in molecular systems and the creation of the Schrödinger cat state. It was theoretically predicted that there are several mechanisms that lead to squeezing of phonon states.

It was found earlier that a sudden frequency change during an electronic Franck–Condon transition leads to special quantum mechanical statistics, called squeezing [2–9], of the molecular vibrations [10–12]. A state is termed "squeezed" if some of its characteristics have less noise than the corresponding quantum noise of the vacuum state. The concept of squeezing turned out to be very fruitful in basic research and implies a lot of promising practical possibilities.

The above-mentioned mechanism of squeezing the vibrational state prompted some controversial discussion in the literature [13–16]. The phenomenon is caused by the change of the frequency of the molecular vibration provided that the transition takes place in a fraction of time negligibly small as compared with the vibrational period. Recently we have shown that phonon squeezing, connected to the finite duration of the excitation pulse, occurs even in the absence of frequency change. This effect would be rather common in ultrashort laser pulse experiments [17–19].

Non-transform-limited pulses, either chirped or incoherent, are very useful in high time resolution spectroscopy [20]. For phonon squeezing, chirped pulses can also be used as shown in Figs. 1 and 2. With a chirped pulse even a Schrödinger cat state can be obtained, as shown in Fig. 2*b*. Advantages of using a chirped pulse are also shown in Fig. 2*b*. As can be seen from the figure, the chirped pulse applied to a periodically oscillating system is equivalent to a double pulse. In such a way, a well controlled chirped pulse may serve a purpose equivalent to a pulse train. The Wigner function corresponding to Fig. 2*b* is shown in Fig. 3. This means that the coherent states are interfering with each other. In such a way we can control a wavepacket by using a chirped pulse instead of an ultrashort pulse.

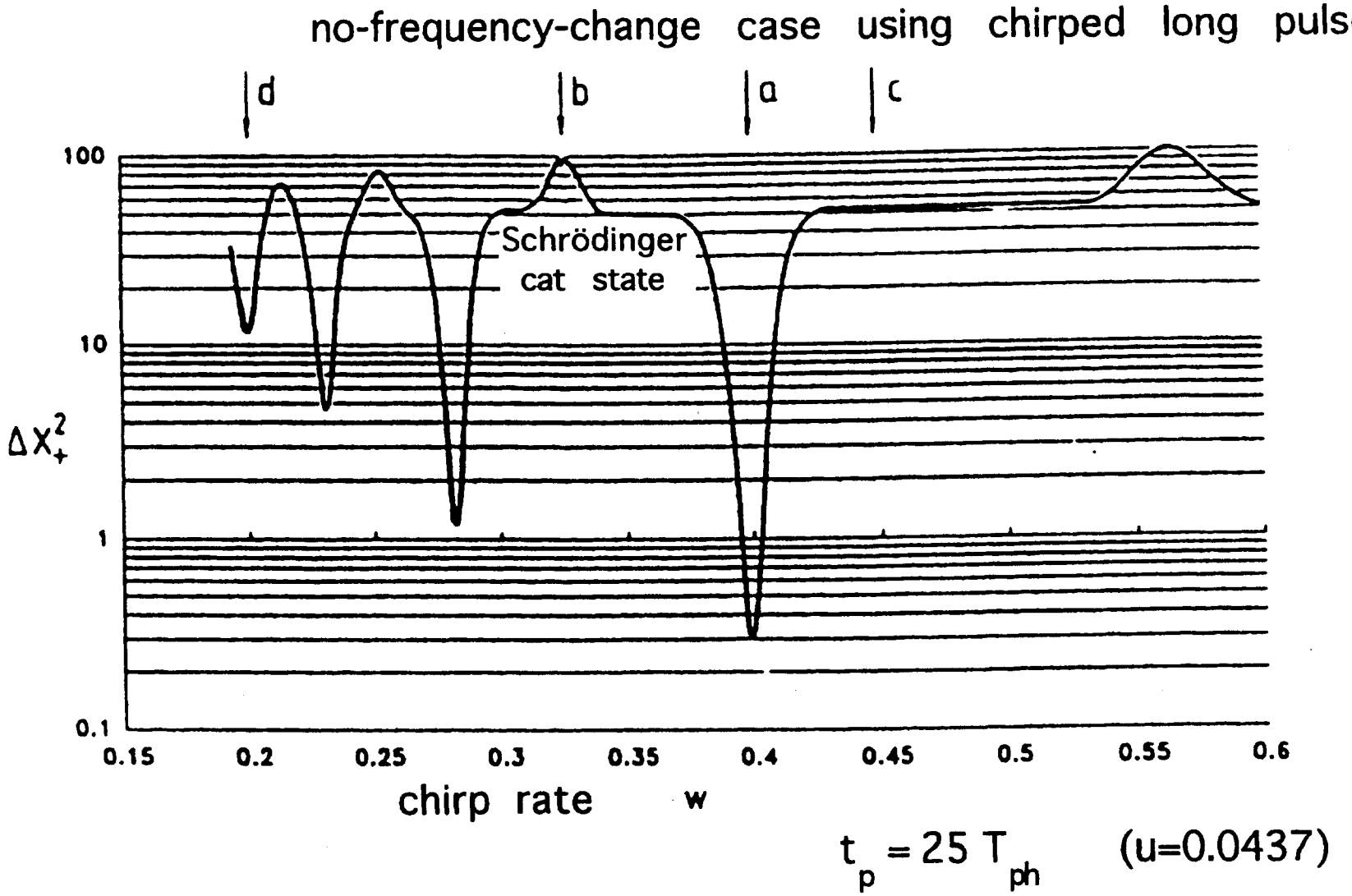

Figure 1. Uncertainty of the quadrature ΔX_+^2 of the phonons (squeezing occurs if ΔX becomes less than unity) after a resonant Franck–Condon transition induced by a chirped pulse of moderate duration

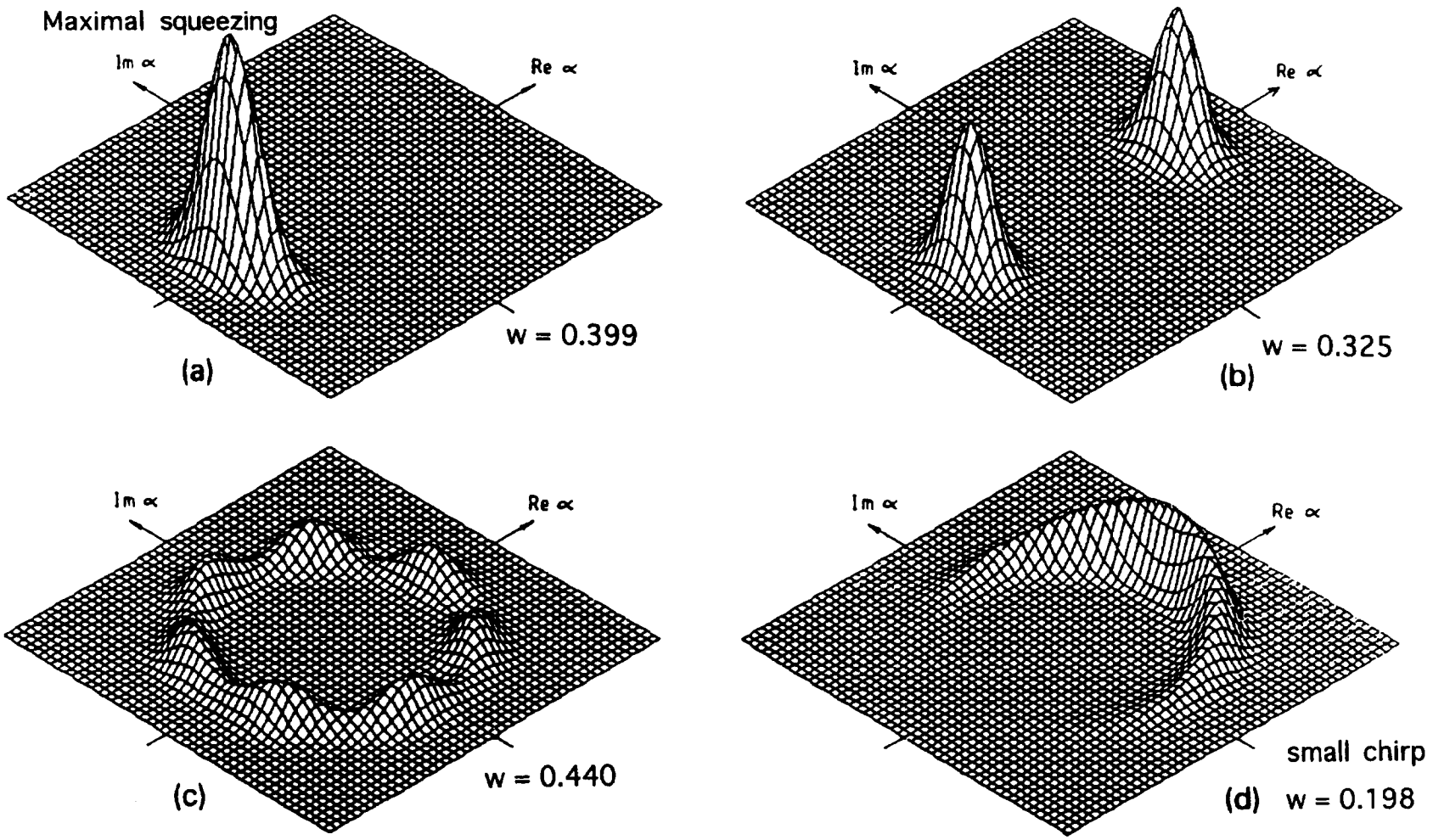

Figure 2. The Q-functions of phonon states after the electronic transition induced by differently chirped pulses. (*a*) The Q-function at the minimal ΔX_+, that is, maximal squeezing (the chirp parameter $w = 0.399$; see marker *a* in Fig. 1). (*b*) The ΔX_- is in its next maximum. (*c*) An intermediate state

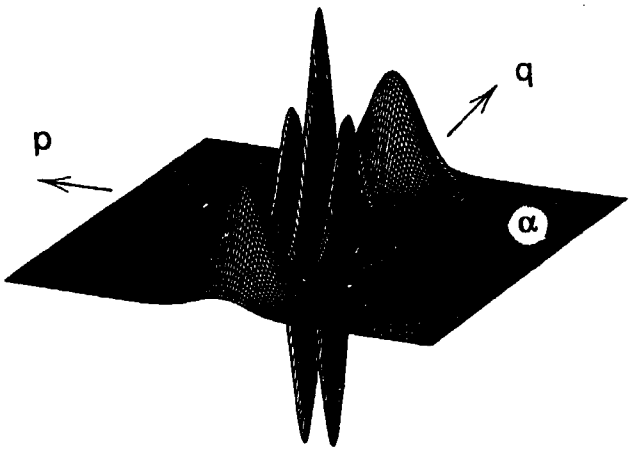

Figure 3. Wigner function corresponding to Fig. 2*b*.

As a method to control wavepackets, alternative to the use of ultrashort pulses, I would like to propose use of frequency-modulated light. Since it is very difficult to obtain a well-controlled pulse shape without any chirp, it is even easier to control the frequency by the electro-optic effect and also by appropriate superposition of several continuous-wave tunable laser light beams.

1. *Physics Today* **43**(5) (1990), Special Issue on Dynamics of Molecular Systems.
2. D. F. Walls, *Nature* **306,** 141 (1983).
3. R. Loudon and P. L. Knight, *J. Mod. Opt.* **34,** 709 (1987).
4. M. C. Teich and B. E. Saleh, *Quantum Opt.* **1,** 153 (1989).
5. L.-A. Wu, H. J. Kimble, J. L. Hall, and H. Wu, *Phys. Rev. Lett.* **57,** 2520 (1986).
6. W. Schleich and J. A. Wheeler, *Nature* **326,** 574 (1987).
7. J. Gea-Banacloche, R. R. Schilcher, and M. S. Zubairy, *Phys. Rev. A* **38,** 3514 (1988).
8. J. Janzky and Y. Yushin, *Phys. Rev. A* **36,** 1288 (1987).
9. C. K. Hong and L. Mandel, *Phys. Rev. A* **32,** 974 (1985).
10. S. Reynaud, C. Fabre, and E. Giacobino, *J. Opt. Soc. Am. B* **4,** 1520 (1987).
11. J. Janzky and Y. Yushin, *Optics Commun.* **59,** 151 (1986).
12. R. Graham, *J. Mod. Opt.* **43,** 873 (1987).
13. H.-Y. Fan and H. R. Zaidi, *Phys. Rev. A* **37,** 2985 (1988).
14. J. Janzky and Y. Yushin, *Phys. Rev. A* **39,** 5445 (1989).
15. H.-Y. Fan and H. R. Zaidi, *Phys. Rev. A* **39,** 5447 (1989).
16. Xi Ma and W. Rhodes, *Phys. Rev. A* **39,** 1941 (1989).
17. J. Janzky, T. Kobayashi, and An. V. Vinogradov, *Optics Commun.* **76,** 30 (1990).
18. W. T. Pollard, S.-Y. Lee, and R. A. Mathies, *J. Chem. Phys.* **92,** 4012 (1990).
19. J. Janzky and An. V. Vinogradov, *Phys. Rev. Lett.* **64,** 2771 (1990).
20. T. Kobayashi, A. Terasaki, T. Hattori, and K. Kurokawa, *Appl. Phys. B* **47,** 107 (1988).

S. R. Jain: When Prof. Rice talks about optimal control schemes, his Lagrange function follows a time-reversed Schrödinger equation. Is it assumed in the variational deduction that the Hamiltonian is time reversal invariant; that is, is it always diagonalizable by orthogonal transformations?

S. A. Rice: Yes, there is time reversal invariance.

S. Mukamel: I would like to make a comment regarding interference effects in quantum and classical nonlinear response functions [1, 2]. Nonlinear optical measurements may be interpreted by expanding the polarization P in powers of the incoming electric field E. To nth order we have

$$P^{(n)}(t) = \int_{-\infty}^{t} d\tau_n \int_{-\infty}^{\tau_n} d\tau_{n-1} \cdots \int_{-\infty}^{\tau_2} d\tau_1 \, E(\tau_n) \cdots E(\tau_1) S^{(n)}(t, \tau_n, \ldots, \tau_1) \quad (1)$$

Quantum mechanically, the nonlinear response function $S^{(n)}(t, \tau_n, \ldots, \tau_1)$ is given by a combination of 2^n terms representing all possible "left" and "right" actions of the various commutators divided by $\hbar^n$. The various terms are given by an $(n+1)$-order correlation function of the dipole operator V (with different time arguments). These terms interfere, and this gives rise to many interesting effects, such as new resonances. The $(1/\hbar)^n$ factor indicates that individual correlation functions do not have an obvious classical limit; however the observables which are given by proper combinations of correlation functions are analytic functions of $\hbar$. The quantum linear response function is given by

$$S_q^{(1)}(t, \tau_1) = \frac{i}{\hbar} [\langle V(t)V(\tau_1)\rangle - \langle V(\tau_1)V(t)\rangle] \quad (2)$$

The classical linear response function can be written using the fluctuation–dissipation theorem as a single term,

$$S_c^{(1)}(t, \tau_1) = -\beta \frac{d}{d\tau_1} \langle V(t)V(\tau_1)\rangle \qquad \beta \equiv (kT)^{-1} \quad (3)$$

Unlike the quantum response (2), which contains an interference of two Liouville space paths, the classical expression (3) contains no inter-

ference and may be directly computed using classical trajectories that sample the initial density matrix.

However, classical *nonlinear* response functions do involve interference between two or more terms. The second-order quantum and classical response functions are given by

$$S_q^{(2)}(t,\tau_2,\tau_1) = \left(\frac{i}{\hbar}\right)^2 [\langle V(t)V(\tau_2)V(\tau_1)\rangle + \langle V(\tau_1)V(\tau_2)V(t)\rangle - \langle V(\tau_2)V(t)V(\tau_1)\rangle - \langle V(\tau_1)V(t)V(\tau_2)\rangle]$$

$$S_c^{(2)}(t,\tau_2,\tau_1) = \beta^2 \frac{d^2}{d\tau_2\, d\tau_1} \langle V(t)V(\tau_2)V(\tau_1)\rangle - \beta \frac{d}{d\tau_1} \langle \omega_{ij} M_{jk}(\tau_2,\tau_1) V(t) V_i'(\tau_2) V_k'(\tau_1)\rangle$$

where $V_j' \equiv \partial V/\partial x_j$ and x_j are the coordinates and momenta. The matrix M, which relates small deviations δx_j to δx_k at different times, is known as the stability matrix. Its elements are defined as

$$M_{jk}(\tau_2,\tau_1) \equiv \left\{ \frac{\partial x_k(\tau_1)}{\partial x_j(\tau_2)} \right\} \tag{4}$$

The stability matrix carries the necessary information related to the vicinity of the trajectory and provides an efficient numerical procedure for computing the response function. It plays an important role in the field of classical chaos; the sign of its eigenvalues (related to the Lyapunov exponents) controls the chaotic nature of the system. Interference effects in classical response functions have a different origin than their quantum counterparts. For each initial phase-space point we need to launch two trajectories with very close initial conditions. [For $S^{(n)}$ we need n trajectories.] The nonlinear response is obtained by adding the contributions of these trajectories and letting them interfere.

It is interesting that the linear response does not depend on M. Nonlinear spectroscopy should therefore be a much more sensitive probe for classical chaos than linear spectroscopy.

1. S. Mukamel, *Principles of Nonlinear Optical Spectroscopy*, Oxford University Press, New York, 1995.

2. S. Mukamel, V. Khidekel, and V. Chernyak, *Phys. Rev. E* **53**, 1 (1996).

S. A. Rice: I would appreciate hearing the comments of Prof. Mukamel concerning the approach to the classical limit from the point of view of his formalism. Is that approach analytic?

S. Mukamel: The nth-order response function is given by a combination of 2^n correlation functions divided by $\hbar^n$. In the classical limit, the combination of correlation functions (but not each one individually) behaves as $\hbar^n$ and $\hbar$ cancels. It is then possible to expand the response function analytically in $\hbar$. As long as we expand a physical quantity (i.e., a response function) rather than a correlation function, the result will be analytic.

E. Pollak: I am not sure I understand the remark by Prof. Mukamel that chaos does not express itself in the linear response regime. The fluctuations of the exact quantum response about the classical will be described in terms of the Gutzwiller summation and will thus reflect the chaos.

S. Mukamel: While there are some signatures of chaos in the linear response, my point is that the nonlinear response carries much more direct and sensitive information. The reason is that the stability matrix enters the nonlinear response directly, reflecting interference of initially close trajectories. Such interference is absent in the linear response.

P. W. Brumer: Prof. Mukamel has emphasized that in examining objects as they approach the classical limit one sees essential singularity behavior or not depending upon the object.

I would like to add to this remark by indicating that we have recently successfully completed a program designed to demonstrate the emergence of classical mechanics from quantum mechanics for dynamics, be it integrable or chaotic. This approach is an extensive generalization of our earlier papers [C. Jaffe and P. Brumer, *J. Chem. Phys.* **82,** 2330 (1985); C. Jaffe, S. Kanfer, and P. Brumer, *Phys. Rev. Lett.* **54,** 8 (1995)], where correspondence requires establishing a relationship, as $\hbar \rightarrow 0$, of the eigenvalues and eigenfunctions of the quantum Liouville operator with the eigenvalues and eigenfunctions of the classical Liouville operator. In addition to producing a completely general approach to classical-quantum correspondence, our approach [J. Wilkie and P. Brumer, *J. Chem. Phys.*, submitted] shows that the classical limit emerges by the elimination of essential singularities.